Relaxin/insulin-like family peptide receptor 4 (Rxfp4) expressing hypothalamic neurons modulate food intake and preference in mice

Author list – Jo E Lewis[1,*], Orla RM Woodward[1,*], Danaé Nuzzaci[1], Christopher A Smith[1], Alice E Adriaenssens[1], Lawrence Billing[1], Cheryl Brighton[1], Benjamin U Phillips[2], John A Tadross[1,3], Sarah J Kinston[4], Ernesto Ciabatti[4], Berthold Göttgens[4], Marco Tripodi[5], David Hornigold[6], David Baker[6], Fiona M Gribble[1,#], Frank Reimann[1,#]

Affiliations:

[1]Wellcome Trust – MRC Institute of Metabolic Science Metabolic Research Laboratories, Addenbrooke's Hospital, Hills Road, Cambridge, CB2 0QQ, UK

[2] Department of Physiology, Development and Neuroscience, University of Cambridge, Cambridge, UK.

[3] Department of Histopathology and East Midlands and East of England Genomic Laboratory Hub, Cambridge University Hospitals NHS Foundation Trust, Cambridge, UK.

[4] Department of Haematology, Wellcome and MRC Cambridge Stem Cell Institute, University of Cambridge, Cambridge, UK

[5] MRC Laboratory of Molecular Biology, Neurobiology Division, Francis Crick Avenue, Cambridge CB2 0QH, UK

[6] Research and Early Development Cardiovascular, Renal and Metabolism (CVRM), BioPharmaceuticals R&D, AstraZeneca Ltd, Cambridge, UK

* These authors contributed equally to this work.

[#] Corresponding authors – acting correspondence: Frank Reimann (email: fr222@cam.ac.uk)

Abstract

Relaxin/insulin-like-family peptide receptor-4 (RXFP4), the cognate receptor for insulin-like peptide 5 (INSL5), has been implicated in feeding behaviour as *Rxfp4* knockout mice display shorter meal durations and reduced high fat diet (HFD) intake. Here, we generated transgenic *Rxfp4*-Cre mice to explore *Rxfp4* expression and physiology. Using this model, we identified *Rxfp4* expression in the central nervous system, including in the ventromedial hypothalamus (VMH). Intra-VMH infusion of INSL5 increased HFD and highly palatable liquid meal intake (HPM) of *ad libitum* fed wildtype mice. Single-cell RNA-sequencing of VMH *Rxfp4*-expressing cells ($RXFP4^{VMH}$) defined a cluster of *Rxfp4*-labelled neurons expressing *Esr1, Tac1* and *Oxtr,* alongside known appetite-modulating neuropeptide receptors (*Mc4r*, *Cckar* and *Nmur2*). Viral tracing demonstrated $RXFP4^{VMH}$ neural projections to the bed nucleus of the stria terminalis, paraventricular hypothalamus, paraventricular thalamus and central nucleus of the amygdala. Utilising designer receptors exclusively activated by designer drugs (DREADDs), we found that whole body chemogenetic inhibition (Di) of *Rxfp4*-expressing cells, mimicking native INSL5-RXFP4 signalling, increased intake of HFD and HPM, whilst activation (Dq), either at whole body level or specifically within the VMH, reduced HFD and HPM intake and altered food preference. Ablating VMH *Rxfp4*-expressing cells recapitulated the lower HFD intake phenotype of *Rxfp4* knockout mice, resulting in reduced body weight. These findings identify a discrete *Rxfp4*-expressing neuronal population as a key regulator of food intake and preference and reveal hypothalamic RXFP4 signalling as a target for feeding behaviour manipulation.

42 **Introduction**

43 Relaxin/insulin-like-family peptide receptor-4 (RXFP4) is the cognate receptor for insulin-like peptide 5
44 (INSL5), a member of the relaxin/insulin-like peptide family(1-3). We previously reported an orexigenic
45 effect of exogenously applied INSL5 in mice(4). More recently, we observed a transient increase in food
46 intake when *Insl5* expressing cells were chemogenetically activated (5). This was only revealed when the
47 dominant anorexigenic action of PYY, co-secreted from the same cell population in the distal large
48 intestine (6), was blocked with a NPY2R antagonist (5). Reports that *Insl5* knockout (*Insl5*$^{-/-}$) mice do not
49 display an observable feeding phenotype and that, in some studies, pharmacological administration of
50 INSL5 (both native and PEGylated forms) failed to increase food intake in lean and obese mice (7, 8), have
51 shed some doubt on whether INSL5 plays a physiologically relevant role in the control of food intake.
52 However, *Rxfp4* knockout (*Rxfp4*$^{-/-}$) mice exhibit shorter meal durations, particularly when fed a high fat
53 diet (HFD), and lack the normal preference for HFD over standard chow diet observed in wildtype mice
54 (4). We therefore consider RXFP4 to be a potential target receptor for the manipulation of feeding
55 behaviour.

56 RXFP4 is a $G_{\alpha i/o}$-coupled receptor identified in 2003 through its homology to relaxin/insulin-like peptide
57 receptor 3, RXFP3 (9, 10). Binding of INSL5 activates downstream signalling pathways including
58 phosphorylation ERK1/2, Akt, p38MAPK and S6RP and reduces cytosolic cAMP levels through inhibition of
59 adenylate cyclase (2). In addition to the selective ligand INSL5, Relaxin-3 can also activate RXFP4,
60 stimulating comparable signalling pathways (2, 11). *Rxfp4* mRNA expression has been reported in the
61 colon, kidney, heart, liver, testes and ovary of both mice and humans (1, 10, 11). To identify and
62 manipulate *Rxfp4*-expressing cells, we developed a new transgenic mouse model in which Cre-
63 recombinase expression is driven by the *Rxfp4* promoter (*Rxfp4*-Cre). Utilising this model, we found clear
64 Cre-dependent reporter expression within the CNS, including the ventromedial hypothalamus (VMH). This

65 contrasts with our previous study, in which we failed to detect *Rxfp4* expression in the central nervous
66 system by qPCR, and in which intracerebroventricular administration of INSL5 failed to increase food
67 intake significantly (4). Revisiting the potential central role of RXFP4 in food intake regulation, we
68 observed that infusion of INSL5 directly into the VMH induced a significant orexigenic response when mice
69 were offered a HFD or a highly palatable liquid Ensure test meal (HPM), but not when offered a standard
70 chow diet. We therefore used the *Rxfp4*-Cre mouse model to explore the role of *Rxfp4*-expressing cells in
71 shaping food intake and preference.

72 **Results**

73 To investigate a possible role of *Rxfp4*-expressing cells in feeding control, we generated a new BAC
74 transgenic mouse (*Rxfp4*-Cre) model in which Cre-recombinase is expressed under the control of the
75 *Rxfp4*-promoter (Fig. 1a). By crossing *Rxfp4*-Cre mice with fluorescent protein reporter mice (e.g. Rosa26
76 fxSTOPfx-EYFP (RXFP4^{EYFP})) (Fig. 1b) we observed *Rxfp4* dependent expression in the colon (Fig. 1c),
77 consistent with previous reports, but also detected reporter expression in the central nervous system
78 (CNS) (Suppl. Fig. 1) by GFP immunohistochemistry. Within the CNS we observed reporter expression in
79 the ventromedial hypothalamus (VMH), the accessory olfactory bulb, septofimbrial nucleus, retrosplenial
80 cortex, and the mammillary body medial and lateral parts, as well as in a lower density of cells in the
81 substantia innominata, cortical and central amygdala, periaqueductal grey, and spinal trigeminal tract of
82 the hindbrain (Suppl. Fig 1). Closer examination of the VMH using RXFP4^{GCaMP3} mice revealed transgene
83 expression in the central and ventrolateral parts (VMHc and VMHvl, respectively) extending into the
84 adjacent tuberal nucleus (TN) (Fig. 1d,e), despite our previously reported failure to amplify *Rxfp4* from
85 hypothalamic cDNA by RT-PCR (4). The VMH is a central hub for the regulation of energy balance and
86 integration of diverse nutritionally regulated hormonal and synaptic inputs, and the adjacent TN has also
87 been implicated in feeding behaviour (12, 13). In the VMH, co-staining with NeuN demonstrated GFP
88 expression in mature *Rxfp4* positive neurons (Fig. 1f). Active transcription of *Rxfp4* mRNA in the adult
89 mouse VMH was confirmed by RNAscope (Fig. 1g,h). To test the functional activity of the RXFP4-INSL5
90 pathway in the *Rxfp4*-expressing cells in the VMH (RXFP4^{VMH}) , we performed real time monitoring of
91 cAMP levels in RXFP4^{VMH} using ex vivo CAMPER (14) imaging in hypothalamic slices from Rxfp4-Cre x
92 CAMPER (RXFP4^{CAMPER}) mice. We found that 14 out of 54 YFP-positive cells showed a clear reduction in
93 the ΔFRET ratio (YFP/CFP), reflecting a reduction in cAMP levels, in response to INSL5 (Fig. 1i), whilst the
94 remaining cells displayed no obvious change in FRET signal in response to INSL5 addition. To test the
95 functional significance of the RXFP4^{VMH} cells in vivo, we treated wildtype ad libitum (AL) fed lean mice with

96 an intra-VMH infusion of INSL5 after a 2h fast. During the light phase, INSL5 had no effect on standard
97 (std) chow intake (Fig.1j) but in mice which were habituated to the appearance of a HFD or HPM for 1
98 hour, treatment with INSL5 significantly increased HFD and HPM intake compared to the vehicle control
99 treatment (Fig.1k,l).

100 As intra-VMH INSL5 significantly modulated feeding behaviour, we further characterised the *Rxfp4*-
101 expressing cells in this region. Initially, we generated a single cell resolution transcriptomic profile of
102 *Rxfp4*-expressing cells in the hypothalamus. Fluorescent cell populations from the hypothalami of twelve
103 RXFP4^{EYFP} mice were purified by FACS and their transcriptomes analysed by scRNA-Seq. After data
104 normalisation, 350 cells passed quality control filtering. Graph-based clustering analysis revealed that the
105 filtered cells separated into five populations (Fig. 2a). Cluster identities were assigned based on the
106 expression patterns of canonical cell-type markers, identifying microglia (*Tmem119*, *Siglech*, *P2ry12*),
107 neuronal cells (*Snap25, Tubb3, Elavl2*) and endothelial cells (*Dcn*, *Hspg2*), together with smaller clusters
108 of macrophages (*Mrc1*, *Mgl2*) and ependymocytes (*Ccdc153*, *Hdc*) (Fig. 2b). As IHC had suggested neuronal
109 *Rxfp4* expression (Fig1f) and hypothalamic neurons are known to modulate feeding behaviour, we
110 analysed the neuronal cluster in more detail, identifying seven subclusters (Fig. 2c). *Rxfp4*-positive
111 neurons expressed markers for both GABAergic (*Slc32a1*) and glutamatergic (*Slc17a6*) cells (Fig. 2d).
112 Cluster 1 was enriched in markers previously associated with an estrogen receptor (*Esr1*)-positive VMHvl
113 neuronal population (15, 16), including preprotachykinin-1 (*Tac-1*), oxytocin receptor (*Oxtr*),
114 cholecystokinin receptor A (*Cckar*), melanocortin 4 receptor (*Mc4r*) and neuromedin U receptor 2 (*Nmur2*)
115 (Fig. 2d), suggesting crosstalk with known food regulatory networks. Receptors for other established
116 feeding-neuromodulators, like glucagon-like peptide-1 receptor (*Glp1r*) and cholecystokinin receptor B
117 (*Cckbr*), were preferentially expressed in cluster 6 (Fig. 2d).

118 We subsequently aimed to establish the neuronal circuitry around RXFP4^{VMH} cells. Anterograde
119 projections were mapped by stereotactically injecting Cre-dependent rAAV8-ChR2-mCherry into the VMH
120 of RXFP4^{GCaMP3}mice (17) (Fig.3a,b). Axonal transport of the ChR2-mCherry fusion protein revealed
121 RXFP4^{VMH} projections to multiple regions including the bed nucleus of the stria terminalis (BNST), preoptic
122 area (POA), anteroventral periventricular nucleus (AVPV), arcuate nucleus (ARC), paraventricular
123 hypothalamus (PVH), central nucleus of the amygdala (CeA), periaqueductal grey (PAG, dorsomedial and
124 lateral) and parabrachial nucleus (PBN, lateral and medial) (Fig. 3c, Suppl. Fig. 3). Retrograde projections
125 were assessed after AVV2-TVAeGFP-oG injection followed by Rab-ΔG-EnvA-mCherry (18) injection 21 days
126 later into the VMH of *Rxfp4*-Cre mice (Fig. 3d). The retrograde monosynaptic transport of Rab-mCherry
127 labelled inputs from several nuclei established in feeding regulation, including the ARC, DMH and PVH
128 (Fig. 3d-f). The neuronal circuitry surrounding RXFP4^{VMH} cells is summarised in Fig. 3g.

129 Due to the previously reported altered feeding patterns and macronutrient preferences of *Rxfp4* knock-
130 out mice (4), we further explored the physiology of the RXFP4^{VMH} population by ablating *Rxfp4*-expressing
131 cells using rAAV-DTA injected into the VMH of RXFP4^{GCaMP3} mice (Fig. 4a). Postmortem histological analysis
132 revealed a >90% reduction in RXFP4^{VMH} cells (identified by GFP immunohistochemistry) across the VMH.
133 In the 8 weeks following the surgery, the RXFP4^{VMHKO} mice gained less body weight compared to the
134 control rAAV-mCherry injected mice (Fig. 4c), when fed with a choice of standard chow and HFD in parallel.
135 Five weeks post-surgery the mice were studied in metabolic cages. RXFP4^{VMHKO} mice had a lower
136 respiratory exchange ratio (RER, Fig. 4d), whilst energy expenditure and ambulatory activity (Fig. 4e,f)
137 were unaffected by ablation. Average 24hr food intake was significantly reduced, a consequence of
138 reduced HFD intake (Fig. 4g). Meal duration was unaffected by treatment, however the interval between
139 meals (Fig. 4i) was significantly increased. These data demonstrate the importance of this neuronal
140 population in governing long-term feeding behaviour.

141 Given that RXFP4^{VHMKO} mice ate less HFD, yet central Insl5 infusion, which we would predict to inhibit
142 RXFP4-expressing neurons, increased HFD intake, we investigated the effects of acute activation or
143 inhibition of *Rxfp4*-expressing cells. Initially we used a whole-body hM4Di DREADD Cre-reporter (RXFP4^{wb-}
144 ^{Di}) to mimic the established RXFP4-signalling via pertussis-toxin sensitive Gi pathways (2) (Fig. 5a). During
145 the light phase, activation of Di in *Rxfp4*-expressing cells using CNO had no measurable effect on food
146 intake in AL fed mice(Fig. 5b). However, when animals were habituated to the appearance of a HFD or
147 HPM for 1 hour during the light phase, CNO application resulted in increased food intake (Fig. 5c,d). These
148 results were consistent with the response to infusion of INSL5 into the VMH. To investigate this further,
149 we gave mice housed in metabolic cages the choice between standard chow and HFD. CNO injection
150 during the light phase significantly increased HFD but not chow intake in RXFP4^{wb-Di} mice (Fig. 5e). This
151 effect was transient (Fig. 5f), consistent with the pharmacokinetics of CNO (19), and occurred without any
152 significant differences in ambulatory activity or energy expenditure compared to the vehicle cross-over
153 control (Suppl. Fig. 4a,b).

154 We next investigated the effects of whole-body hM3Dq Cre-reporter activation in *Rxfp4*-expressing cells
155 (RXFP4^{wb-Dq}) (Fig. 6a). After a 2 h brief fast, to enhance feeding motivation, activation of Dq in *Rxfp4*-
156 expressing cells at the onset of the dark phase had no measurable effect on the food intake of mice offered
157 only standard chow (Fig. 6b). However, when RXFP4^{wb-Dq} animals were habituated to the appearance of
158 HFD or a HPM for 1 hour at the onset of the dark phase, activation of Dq expressing cells with CNO resulted
159 in a marked reduction in HFD or HPM intake (Fig. 6c,d). These results were consolidated in AL fed animals
160 tested in metabolic cages with parallel access to standard chow and HFD. RXFP4^{wb-Dq} activation in AL fed
161 animals at the onset of the dark phase had no effect on standard chow intake, but significantly and
162 transiently reduced HFD consumption (Fig. 6e,f). RXFP4^{wb-Dq} activation also attenuated the increase in
163 energy expenditure associated with the onset of the dark phase, however, there was no effect on
164 ambulatory activity (Suppl. Fig. 4c,d).

165 To probe whether *Rxfp4*-expressing cells play a role in the motivational aspects of feeding, we calorically
166 restricted male RXFP4$^{wb\text{-}Dq}$ animals to 95% body weight and placed them in operant chambers. Mice were
167 tested with a fixed ratio (FR) schedule, requiring 5 nose pokes to release a food reward (liquid Ensure), or
168 a progressive ratio (PR) schedule requiring increasing number of nose pokes for each subsequently earned
169 reward (in this case, +4, i.e. 1, 5, 9, 13, etc). RXFP4$^{wb\text{-}Dq}$ mice treated with CNO completed fewer attempts
170 under FR to earn individual Ensure rewards (Fig. 6g). Under a PR schedule, they exhibited a reduced
171 breakpoint, i.e. CNO-treated mice stopped working for the HPM-reward at lower ratios than when
172 receiving vehicle treatment (Fig. 6h). In an effort related choice (ERC) paradigm, where animals had the
173 choice of working for a HPM (FR8, liquid Ensure) or consuming freely available standard chow, CNO
174 treatment reduced HPM consumption (Fig. 6i). However, animals consumed similar amounts of standard
175 chow and displayed otherwise normal behaviour (supplementary video 1), suggesting that activation of
176 *Rxfp4*-expressing cells reduced motivation for the HPM rather than inducing generalised malaise.

177 To assess whether the *Rxfp4*-expressing population in the VMH is involved in the feeding phenotype
178 observed in RXFP4$^{wb\text{-}Dq}$ mice, the effect of acute chemogenetic manipulation of RXFP4^{VMH} neuron activity
179 on food intake was investigated. Male and female *Rxfp4*^{GCAMP3} mice received bilateral VMH injections of
180 Cre-dependent hM3Dq-expressing rAAVs (rAAV-hSyn-DIO-hM3D(G)q-mCherry) designed to preferentially
181 target neurons, to produce RXFP4^{VMHDq} mice (Fig. 7a). Targeting efficiency was subsequently determined
182 by immunohistochemistry (Fig. 7b), or in a subset by fluorescent microscopy in live slices (see below). All
183 mice demonstrated robust transduction that was limited to the target region. To confirm the functional
184 activation of these RXFP4^{VMHDq} neurons, we generated ex vivo brain slices from a subset of RXFP4^{VMHDq}
185 mice (Fig. 7c). Calcium imaging demonstrated that ex vivo treatment with CNO activated
186 mCherry/GCaMP3 positive RXFP4^{VMHDq}, stimulating an increase in the frequency of calcium oscillations
187 and an increase in GCaMP3 fluorescence in *Rxfp4*-expressing somas (Fig. 7c,d).

188 The effect of chemogenetic activation of this cell population in vivo on food intake was studied in a
189 crossover design. In chow fed mice, and in line with RXFP4$^{wb\text{-}Dq}$ animals, CNO treatment of RXFP4^{VMHDq}
190 mice had no effect on standard chow intake at the onset of the dark phase (Fig. 7e). When animals were
191 habituated to the appearance of a HFD or HPM at the onset of the dark phase, CNO resulted in a significant
192 reduction in food intake (Fig. 7f,g). When offered HFD and chow diet in parallel in metabolic cages, CNO
193 significantly reduced intake of the HFD whilst intake of standard chow was not altered, resulting in an
194 overall reduced caloric intake (Fig. 7h). As seen with RXFP4$^{wb\text{-}Dq}$ animals, this was a transient effect no
195 longer apparent in the 2nd hour post CNO administration (Fig. 7i). CNO had no effect on energy
196 expenditure or ambulatory activity in these RXFP4^{VMHDq} animals (Suppl. Fig. 4e,f).

197

198 **Discussion**

199 The *Rxfp4*-Cre mouse model generated in this study has enabled the identification of central *Rxpf4*-
200 expressing cells, and aided the transcriptomic, functional and anatomical characterisation of a
201 hypothalamic *Rxfp4*-expressing neuronal population. We show that *Rxfp4* is expressed in key feeding
202 centres of the brain, including neurons of the VMH. Ex vivo CAMPER imaging revealed that INSL5 reduces
203 cAMP levels in *Rxfp4*-expressing VMH neurons and central administration of INSL5 into the VMH increased
204 HFD and HPM intake in lean AL fed mice in vivo. Mimicking the native physiology of INSL5-RXFP4 via Di
205 recapitulated these results, whereas chemogenetic cell activation via Dq suppressed HFD and HPM intake.
206 Selective chemogenetic activation of *Rxfp4*-expressing cells in the VMH alone (targeted via rAAV-Dq) also
207 suppressed HFD and HPM intake, reflecting their position in brain circuits implicated in homeostatic and
208 hedonic regulation of food intake(20). Ablation of the VMH *Rxfp4*-positive cell population resulted in
209 lower HFD consumption and body weight, mirroring the phenotype of global *Rxfp4* knockout mice (4) and
210 supporting the conclusion that *Rxfp4* neurons in the VMH play a role in the physiological drive to consume
211 highly palatable foods. Overall, these data identify hypothalamic RXFP4 signalling as a key regulator of
212 food intake and preference.

213 *Rxfp4* expression has been difficult to localise due to low mRNA expression levels and the lack of suitable
214 verified antibodies. *Rxfp4* expression was previously reported in the colon (4) and in enteroendocrine
215 tumor cell lines (21, 22). In contrast to our previous report (4), we detected *Rxfp4* mRNA in the
216 hypothalamus (Fig. 1g,h) and found substantial *Rxfp4*-dependent reporter expression in multiple brain
217 regions, with distinct *Rxfp4*-expressing cell populations in the accessory olfactory bulb, RSC, VMHvl, and
218 mammillary body (Suppl. Fig. 1). While it could be argued that this reflects lineage tracing from *Rxfp4*-
219 positive precursor cells, the detection of *Rxfp4* mRNA by RNAscope, the activation of Cre-dependent
220 rAAV-constructs when stereotactically injected into the adult VMH, the cAMP responsiveness of *Rxfp4*-
221 positive cells to locally-perfused INSL5 in slice preparations, and the effect of stereotactically injected

222 INSL5 on feeding behaviour, confirm active *Rxfp4*-promoter activity and consolidate active RXFP4
223 expression and function in the adult mouse brain (Fig. 1g,h, Fig. 7b).

224 To characterise the transcriptomic profile of hypothalamic *Rxfp4*-expressing cells we performed scRNA-
225 Seq. Although some cells will have been lost and some genes may have exhibited altered expression
226 during the cell dissociation and sorting process, the results allowed us to cluster *Rxfp4*-expressing cells
227 into several subpopulations each characterised by a profile of cell-specific marker genes (Fig. 2a,b). *Rxfp4*
228 was identified in microglia, ependymocytes and endothelial cells that potentially constitute the blood
229 brain barrier, suggesting that INSL5 may additionally exert effects on non-neuronal cells(23). Clustering of
230 the *Rxfp4*-expressing neuronal population indicated a predominance of glutamatergic neurons with few
231 GABAergic clusters (Fig 2d). Cluster 6 is of note given the expression of *Glp1r*, *Cckbr*, *Sstr1* and *Sstr2*,
232 suggesting an overlap with other known appetite-modulating gut peptide receptors. The cocaine- and
233 amphetamine-regulated transcript (*Cartpt*), expressed in cluster 3, and cannabinoid receptor 1 (*Cnr1*),
234 expressed in clusters 1, 4 and 5, (Fig 2d, Suppl. Fig. 3) have also been implicated in energy homeostasis(24,
235 25). Cluster 1 displayed markers of a VMHvl *Esr1* population (*Esr1, Pgr, Tac1, Cckar, Rprm* and *Oxtr*)
236 previously associated with food intake and energy expenditure(12, 15, 16). However, chemogenetic
237 activation of RXFP4^{VMHDq} neurons did not result in increased energy expenditure or ambulatory activity,
238 contrasting with the previously described Esr1^{VMHDq} phenotype(16). The role of RXFP4^{VMH} cells in feeding
239 regulation is further suggested by the co-expression of the neuropeptide receptors *Mc4r* and *Nmur2.*
240 MC4R activation has been linked to suppressed food intake through regulation of *Bdnf* expression in the
241 VMH (26) – *Bdnf* was co-expressed in cluster 1 neurons in our dataset (Fig. 2d). Acute administration of
242 NMUR2 agonists have been shown to decrease feeding, with one agonist being somewhat selective to
243 HFD intake regulation (27), mirroring RXFP4^{VMHDq} cell activation (Fig 7).

244 Mapping of the retrograde inputs to and anterograde projections from the *Rxfp4*-expressing cells in the
245 VMH revealed a distinct neural circuitry surrounding this hypothalamic population. While we aimed to
246 target the VMHvl specifically during stereotactic injections, disparities between current mouse brain
247 atlases make it difficult to distinguish the VMHvl from the adjacent VMHc and TN, which have also been
248 implicated in feeding behaviour (13, 30) . It is therefore possible that some *Rxfp4*-expressing cells in the
249 VMHc and TN were transfected by the viral vectors and acted as starter cells in these tracing experiments.
250 The *Rxfp4*-expressing population we targeted is therefore best described as RXFP4^{VMH}. Monosynaptic
251 inputs to RXFP4^{VMH} cells were labelled predominantly from brain regions involved in homeostatic
252 regulation of food intake such as the ARC, PVH and LHA (Fig. 3f). Within the ARC, two populations of
253 neurons have been intensely studied with regards to feeding regulation: pro-opiomelanocortin
254 (POMC)/cocaine- and amphetamine-regulated transcript (CART)-expressing neurons inhibit food intake
255 while Agouti-Related Peptide (AgRP)/neuropeptide Y (NPY)-expressing neurons stimulate food intake.
256 These neurons integrate nutritional and hormonal signals from the periphery and send projections to
257 multiple brain regions including the VMH (31). Although the VMH is not thought to be the main target of
258 arcuate POMC projections (32), the co-expression of *Mc4r* in the RXFP4^{VMH} neurons suggests that POMC
259 neurons may be part of the ARC innervation of RXFP4^{VMH} neurons.

260 RXFP4^{VMH} cells predominantly project onto regions associated with reward and motivation-related
261 behaviours (Fig. 3c, Suppl. Fig. 3) such as the BNST, POA, CeA, paraventricular thalamic nucleus (PVT) and
262 ventral tegmental area (VTA) (33-35), potentially underlying our finding that chemogenetic activation of
263 *Rxfp4*-expressing cells in RXFP4$^{wb\text{-}Dq}$ mice reduced an animal's drive to seek out and work for a highly
264 palatable food reward (Fig 6g-i). Taken together, these data suggest that *Rxfp4*-expressing cells may
265 influence motivation and reward-related behaviour via regulation of central reward signalling pathways.
266 RXFP4^{VMH} cells also send projections to the PAG and PBN, two integration sites responsible for relaying
267 sensory information between the forebrain and hindbrain and coordinating behaviour in response to

268 various stimuli including metabolic, gustatory and nociceptive inputs (36-38). This RXFP4^{VMH} projection
269 map aligns with previously identified projection regions from the VMHvl and SST-expressing cells in the
270 TN (13, 39). Interestingly, all retrograde-labelled input regions also received projections from RXFP4^{VMH}
271 cells suggesting a high level of bidirectional connectivity within the RXFP4^{VMH} signalling network (Fig. 3g).
272 Similar bidirectional connectivity has been shown for an *Esr1*+ve VMHvl population (39). The RXFP4^{VMH}
273 neural network established in the present study suggests these cells may integrate metabolic and
274 nutritional cues either directly or via other hypothalamic regions and regulate the reward system to
275 influence ingestive behaviours. The low number of RXFP4^{VMH} input regions compared to projection regions
276 suggests these cells may comprise an early node in this network.

277 Inhibition of *Rxfp4*-expressing cells via direct intra-VMH infusion of INSL5 or whole body Di acutely
278 increased intake of both a HFD and a HPM in the home cage and when animals were offered a choice of
279 standard laboratory chow and HFD in metabolic cages, without altering energy expenditure and activity
280 in both male and female mice (Fig 1j,k, Fig 5, Suppl. Fig 4a,b). This is consistent with our previous
281 demonstration that INSL5 administration increased food intake (4, 5). Activation of Di receptors should,
282 at least in part, mimic the $G\alpha_{i/o}$ coupling of RXFP4 (2). By contrast, activation of *Rxfp4*-expressing cells with
283 Dq produced a robust suppression of HFD and HPM intake (Fig 6). Targeting the RXFP4^{VMH} population with
284 an rAAV-Dq reporter recapitulated the findings with the whole body-Dq approach (Fig. 7). Whilst any of
285 the identified *Rxfp4*-expression sites could participate in the feeding phenotype of the global DREADD
286 reporter mice, the VMH-specific rAAV-Dq reporter phenotype indicates that this hypothalamic population
287 either underlies or at least contributes to the observed anorexigenic effects in the RXFP4$^{wb\text{-}Dq}$ model.

288 Our data suggest that activation of *Rxfp4*-expressing cells in the VMH suppresses the consumption and
289 drive to work for calorie dense HFD and HPM. The importance of the VMH in the regulation of feeding
290 and metabolism has been disputed (reviewed in (40)). Initial studies suggested the VMH might be a

291 “satiety centre”, as VMH-lesioned rats, particularly females, over-consumed a HFD when fed AL (41),
292 despite being seemingly less willing to work for food on a fixed ratio lever-pressing paradigm (42). The
293 observed hyperphagia has subsequently been linked to additional damage to adjacent hypothalamic
294 structures (see King 2006(40) for discussion), while the reduced motivation was not observed when rats
295 were trained pre-operatively, suggesting that the VMH lesion may have altered “trainability” rather than
296 feeding motivation (40, 43). Lesioning studies, whilst informative, lack cellular precision and damage
297 neural connections to other feeding centres within the brain. More recent work employing
298 immunohistochemistry, RNA sequencing, chemogenetics and neuronal projection mapping, has
299 demonstrated that the VMH consists of anatomical subdivisions made up of distinct cell populations(15,
300 44, 45). Functional studies suggest neurons in the central and dorsomedial VMH regulate feeding, energy
301 expenditure and glucose homeostasis (30, 46), while the VMHvl is more frequently implicated in the
302 control of social and sexual behaviours(45, 47, 48). However, several studies have demonstrated the
303 involvement of VMHvl neurons in energy expenditure and feeding behaviour (12, 49). Increases in physical
304 activity have been observed following chemogenetic activation of NK2 homeobox transcription factor 1
305 (*Nkx2-1*)-expressing neurons in the VMHvl of female rats, while knockout of *Nkx2-1* in the VMHvl leads to
306 decreased physical activity and thermogenesis (50). Furthermore, chemogenetic activation of *Esr1*-
307 expressing VMHvl neurons was found to stimulate physical activity and thermogenesis in both sexes (16).
308 *Esr1* signalling in the VMHvl was previously demonstrated to influence food intake, energy expenditure
309 and glucose tolerance as VMHvl-restricted knockdown of *Esr1* resulted in increased food intake,
310 decreased physical activity and thermogenesis, reduced glucose tolerance and obesity in female rats (12).
311 Activation of RXFP4^{VMHDq} neurons reduced HFD and HPM intake but had no effect on chow intake, energy
312 expenditure or ambulatory activity (Fig. 7, Suppl. Fig. 4e,f). This, alongside the transcriptomic profile and
313 neural circuitry of RXFP4^{VMH} neurons, suggests that these neurons comprise a distinct VMH population
314 modulating food intake and preference based on the rewarding aspects of food rather than the

315 homeostatic food intake or energy expenditure responses observed during chemogenetic manipulation
316 of other VMH populations.

317 We recognise several limitations to this study. First, the exact classification of *Rxfp4*-expressing brain
318 regions is difficult given the disparities between current brain atlases. Whilst we aimed to target *Rxfp4*-
319 expressing cells in the VMHvl, the inexact nature of stereotactic injections may have resulted in additional
320 targeting of neurons in adjacent VMHc, LHA and TN regions, which may have contributed to the food
321 intake phenotype of RXFP4^{VMHDq} mice. The fact that only a subset of Rxfp4^{CAMPER} neurons responded to
322 INSL5 in acute slices likely reflects technical limitations of this preparation. The similarities of the feeding
323 outcomes of intraparenchymal INSL5 in WT mice and CNO application in Rxfp4^{VMHDq} mice together with
324 RNAscope confirmation of Rxfp4-Cre labelled VMH neurons makes the alternative explanation of
325 substantial additional off target Cre-expression unlikely, but we cannot fully rule this out. It is also
326 uncertain whether INSL5 is the endogenous ligand acting on *Rxfp4*-expressing cells in the brain. We have
327 previously been unable to identify *Insl5*-expressing cells in the mouse brain (5) and there is no evidence
328 that INSL5 can cross the blood brain barrier. In addition, relaxin-3 also activates RXFP4 (2), is expressed in
329 the mouse brain and is orexigenic (51), hence it is possible that relaxin-3 is involved in central RXFP4
330 action. The viral tracing techniques used to decipher the RXFP4^{VMH} neuronal network also have some
331 limitations. In the retrograde tracing experiments, it was difficult to detect rAAV-GFP immunoreactive
332 cells, making it hard to confirm the exact starter cells in this experiment. Furthermore, while the ChR2-
333 mCherry construct is preferentially targeted to axon terminals, it is possible that some of the mCherry-
334 labelled fibres in adjacent regions, such as the ARC, are in fact dendrites (52) which may underlie our
335 inability to detect retrograde-only labelled regions. Nevertheless, we have been able to identify distinct
336 regions that project onto and receive projections from *Rxfp4*-expressing cells in the VMH that connect
337 these cells to known feeding-related neural networks. Finally, it is difficult to explain apparently similar
338 outcomes of acute chemogenetic activation and chronic ablation of RXFP4^{VMH} neurons, both resulting in

339 reduced HFD consumption. The chronic ablation outcome would be compatible with a positive valence of
340 Rxfp4^{VMH} neurons, whilst the acute Dq experiment would be compatible with a negative valence of the
341 same neurons on HFD consumption, and both interpretations would be compatible with the response to
342 acute parenchymal Insl5 and the phenotype of Rxfp4-knock-out mice. Whilst we are currently unable to
343 distinguish these two interpretations, we nevertheless establish Rxfp4^{VMH} neurons as integral players in a
344 complex neural network consuming highly palatable food consumption.

345 In summary, we have characterised a previously unrecognised population of ventromedial hypothalamic
346 cells that express *Rxfp4* in mice, identified projections in homeostatic and hedonic feeding centres in the
347 CNS, and demonstrated that acute manipulation of these cells modulates HFD/HPM intake without
348 affecting chow intake or energy expenditure. Together, these findings suggest *Rxfp4*-expressing neurons
349 in the VMH are key regulators of food preference and represent a target for the modulation of feeding
350 behaviour.

351

352 **Methods**

353 **Animals**
354
355 All experiments were performed under the UK Home Office project licences 70/7824 and PE50F6065 in
356 accordance with the UK Animals (Scientific Procedures) Act, 1986 and approved by the University of
357 Cambridge Animal Welfare and Ethical Review Body. All mice were from a C57BL/6 background and were
358 group-housed and maintained in individual ventilated cages with standard bedding and enrichment in a
359 temperature and humidity controlled room on a 12h light:dark cycle (lights on 7:00) with *ad libitum* (AL)
360 access to food (Scientific Animal Food Engineering) and water unless otherwise stated. Groups were
361 randomised by body weight and the researcher was blinded to treatment.

362

363 **Mouse models**

364 To express Cre recombinase under the control of the *Rxfp4* promoter, we replaced the sequence between
365 the start codon and the stop codon in the single coding exon of *Rxfp4* in the murine-based BAC RP24-72I4
366 (Children's Hospital Oakland Research Institute) with iCre (53) sequence using Red/ET recombination
367 technology (GeneBridges) (Fig 1A). The resulting BAC was used to create BAC-transgenic mice – of four
368 initial founders, two passed the transgene to their offspring; both resulting lines showed similar Cre-
369 reporter expression and one line, Rxfp4-73, was used throughout this manuscript (see Suppl. methods 1
370 for further information). Several Cre-reporter transgenes, in which expression is only activated after
371 removal of a fxSTOPfx cassette, were used, resulting in expression of EYFP (54), Dq , Di (55), GCaMP3 (56),
372 or tdRFP (57), respectively.

373

374 **Viral injections**

375 Viral injections were performed in male and female *Rxfp4*-Cre mice aged between 9 and 16 weeks. The
376 surgical procedure was performed under isoflurane anaesthesia, with all animals receiving Metacam prior
377 to surgery. Mice were stereotactically implanted with a guide cannula (Plastics One) positioned 1mm
378 above the VMH (A/P: -1.7 mm, D/V: -4.5 mm, M/L: +/- 0.75 mm from bregma). Bevelled stainless steel
379 injectors (33 gauge, Plastics One) extending 1mm from the tip of the guide were used for injections. For
380 anterograde viral tracing experiments, 200 nL rAAV-DIO-ChR2-mCherry (Addgene, 20297-rAAV8,
381 1.9×10^{13} vg/ml) was injected unilaterally at 75 nL/min. Mice were culled three weeks after injection. For
382 retrograde viral tracing experiments, AVV2-FLEX-TVAeGFP-2A-oG (rAAV2-TVAeGFP-oG) and Rabies-ΔG-
383 EnvA-mCherry (Rab-ΔG-EnvA-mCherry) viruses were generated by Ernesto Ciabatti (MRC Laboratory of
384 Molecular Biology, Cambridge). Mice were injected unilaterally with 200 nL AVV2-TVAeGFP-oG ($1x10^{12}$
385 vg/mL) at 75 nL/min followed by 500 nL Rab-ΔG-EnvA-mCherry ($2x10^{9}$ iu/mL) at 75 nL/min three weeks
386 later. Mice were culled seven days after the second injection. For the $RXFP4^{VMHKO}$ studies, 200 nL ssAAV9-
387 hEF1α-dlox-DTA(rev)-dlox-WPRE-hGHp(A) (rAAV-DTA: ETH VVF, $6.2x10^{12}$ vg/mL) or AAV2-hSyn-DIO-

388 mCherry (rAAV-mCherry: Addgene, 50459-AAV2, $4x10^{12}$ vg/mL) was injected bilaterally at 75 nL/min and
389 mice were allowed 2 weeks recovery prior to testing. For phenotyping experiments, 200nL rAAV8-
390 hM3D(G)q-mCherry (Addgene 44361-rAAV8, $4x10^{12}$ vg/mL) was injected bilaterally at 50nl/min and mice
391 were allowed 2 weeks recovery prior to testing.

392

393 **Intra-VMH infusion**

394 Mice were stereotactically implanted with a guide cannula (Plastics One) positioned 1mm above the VMH
395 (A/P: -1.7 mm, D/V: -4.5 mm, M/L: +/- 0.75 mm from bregma). Bevelled stainless steel injectors (33 gauge,
396 Plastics One) extending 1mm from the tip of the guide were used for infusions in free-moving mice. An
397 intra-VMH cannula was placed under isoflurane anaesthesia and the animals was given 1 week to recover.
398 Mice were given AL access to standard (std) chow.

399

400 **Food intake**

401 Food intake studies were performed in a cross-over design, on age-matched groups, a minimum of 72
402 hours apart. Mice were administered vehicle or INSL5 (5ug/animal, Phoenix Biotech, 035-40A) at 12:00-
403 15:00 following a 2h fast. Food was weighed 1h post-injection. For experiments assessing the effect of
404 global RXFP4 Di and Dq activation, animals were singly housed prior to the experiment. Mice were
405 administered 1mg/kg CNO (Sigma, C0832) or an equivalent volume of vehicle containing a matched
406 concentration of DMSO (Sigma, D2650). For light phase activation, animals were injected with vehicle or
407 CNO at 11:00 (± 30mins) following a 2h fast. Food was weighed at 1h post-injection. For dark phase
408 activation, animals were injected with vehicle or CNO at 19:00 at the onset of the dark phase following a
409 2h fast. Food was weighed at 1h post-injection. In trials with a high fat diet (HFD) and a highly palatable

410 meal (HPM, liquid Ensure, Abbott Laboratories, 353-3601), mice were habituated to the appearance of
411 the test meal for 1 hour (5 days per week) for two weeks prior to testing.

412

413 **Operant chambers**

414 Twelve male RXFP4$^{wb\text{-}Dq}$ mice (weighed 3 times weekly) were food restricted to maintain 95% body weight
415 for two weeks prior to training and testing in standard mouse Bussey-Saksida touchscreen chambers
416 (Campden Instruments Ltd, Loughborough, UK). Training and testing procedures were conducted as
417 previously described (58). Briefly, mice were trained to touch a screen for a reward (the HPM, 20 µL) under
418 a fixed ratio (FR) schedule for 2 weeks, progressing from FR1 to FR5 (training deemed successful when the
419 animal earnt 30 rewards within 1 hour), followed by testing. Mice then progressed to progressive ratio
420 (PR, increment +4 i.e. 1, 5, 9, 13, etc), where the breakpoint was defined as the last reward earned before
421 5 minutes elapsed without operant response. Following testing of the breakpoint, mice progressed to the
422 effort related choice schedule (ERC) - mice were trained on FR8, with the addition of standard chow to
423 the operant arena. Once animals successfully earned 30 rewards within 60 minutes, testing was
424 undertaken. The 60-minute training and testing sessions took place at the same time each day (between
425 10:00-13:00).

426

427 **Metabolic cages**

428 Animals were acclimated to metabolic cages prior to study and data collection. Oxygen consumption and
429 carbon dioxide production were determined using an indirect calorimetry system (Promethion, Sable
430 Systems, Las Vegas, NV). The system consisted of 8 metabolic cages (similar to home cages), equipped
431 with water bottles and food hoppers connected to load cells for continuous monitoring, in a temperature
432 and humidity-controlled cabinet. The respiratory exchange ratio (RER) and energy expenditure (via the
433 Weir equation) were calculated, whilst ambulatory activity was determined simultaneously. Raw data

434 were processed using ExpeData (Sable Systems). Animals were exposed to standard chow and a HFD
435 during metabolic assessment or standard chow.

436

437 **CAMPER and calcium imaging**

438 Mice were anesthetized using sodium pentobarbital at a dose of 180mg/kg (Dolethal, Vetoquinone). A
439 laparotomy was then performed, the heart exposed and the animals were intracardiacally perfused with
440 oxygenated High-Mg^{2+}/low Ca^{2+} ice-cold artificial cerebrospinal fluid (perfusion solution; composition in
441 mM: 2.5 KCl, 200 sucrose, 28 $_{NaHCO3}$, 1.25 NaH_2PO4, 8 Glucose, $7MgCl_2$, 0.5 $CaCl_2$; pH 7.4). The brain was
442 extracted from the skull and immersed in oxygenated perfusion solution. 250 μm thick slices of the
443 hypothalamus containing the VMH were cut on a Vibratome (Leica) and placed in a recovery solution (in
444 mM: 3 KCl, 118 NaCl, 25 $NaHCO_3$, 1.2 $NaH2_PO_4$, 2.5 Glucose, 7 $MgCl_2$, 0.5 $CaCl_2$; pH 7.4) at 34 ^oC for 30 min.
445 Sections were then transferred to standard ACSF (in mM: 3 KCl, 118 NaCl, 25 $NaHCO_3$, 10 Glucose, $1MgCl_2$,
446 $CaCl_2$; pH7.4) at room temperature for 1h before recording. All solutions were continuously bubbled with
447 95% O_2/5% CO_2.

448 Imaging was performed using a Zeiss Axioskop2 FS Plus microscope. Slices were immobilised in a glass
449 bottom chamber using a slice anchor (Warner instruments) and imaged using a 40x water immersion
450 objective. For CAMPER imaging, $RXFP4^{CAMPER}$ neurons of the VMH were excited using a LED light source
451 (Dual Optoled, Cairn Research) at 435 for 50ms every 3 seconds and CFP and YFP emission were
452 simultaneously recorded after passing through an optosplit (Cairn; 465-505 and 525-600 nm,
453 respectively). . . For Ca^{2+} imaging, $RXFP4^{GCaMP3}$ neurons were excited at 470 nm for 75 ms every 2 s and
454 emission from 500-550 nm was captured. Images were captured using a charged-coupled camera (Evolve
455 512 Delta, Photometrics), acquisitions were saved and data logged using Metamorph software (Molecular
456 Devices). Slices were continuously superfused with room temperature standard ACSF at a flow rate of 1

457 mL per minute. All drugs were added directly in standard ACSF. CNO (15 μM, C0832), IBMX (100 uM,
458 I7018) and forskolin (10 uM, F6886) were purchased from Sigma. INSL5 (100 nM, 035-40A) was purchased
459 from Phoenix Biotech.

460 Regions of interest (ROIs) and an area determined for background fluorescence were outlined for each
461 image and the mean pixel intensity extracted for each ROI. The mean intensity of the background was
462 subtracted from each ROI. For CAMPER imaging, the fluorescence energy transfer ratio (ΔFRET) of the
463 mTurquoise FRET donor (CFP) and Venus FRET acceptor (YFP) was calculated and is presented on a reverse
464 axis. INSL5 responses were measured by calculating the percentage change in ΔFRET between the
465 maximum IMBX response and the maximum INSL5 response. For Ca^{2+} imaging, fluorescence intensity of
466 the GCaMP3 is presented as $\Delta F/F_0$ with F_0 being the mean intensity for 5 min before stimulus and ΔF the
467 fluorescence intensity F minus F_0. Responses were observed on raw and $\Delta F/F_0$ traces and quantified by
468 calculating areas under the curve (AUCs) over 5 min before the stimulus for the ACSF condition and over
469 5 minutes after the stimulus for the treated conditions. Cells were considered activated by stimuli if the
470 AUC increased by 25% after treatment compared to the AUC before treatment.

471

472 **Immunohistochemistry**

473 Colonic tissues were fixed in 4% paraformaldehyde (PFA), dehydrated in 15% and 30% sucrose, and frozen
474 in OCT embedding media (CellPath, Newtown, U.K.). Cryostat-cut sections (8-10μm) were mounted
475 directly onto poly-L-lysine-covered glass slides (VWR, Leuven, Belgium) by the Institute of Metabolic
476 Science Histology Core. Slides were incubated for 1hr in blocking solution containing 10% goat or donkey
477 serum. Slides were stained overnight at 4°C with primary antisera (table 1) in PBS/0.05% Triton X-100/10
478 % serum. Slides were washed with blocking solution and incubated with appropriate secondary antisera
479 (donkey or goat Alexa Fluor® 488, 546, 555, 633 or 647; Invitrogen) diluted 1:400 and Hoechst diluted

480 1:1500 for 1 hr. Control sections were stained with secondary antisera alone. Sections were mounted with
481 Prolong Gold (Life Technologies) or hydromount (National Diagnostics, Atlanta, Georgia, USA) prior to
482 confocal microscopy (Leica TCS SP8 X, Wetzlar, Germany). Quantification of cell number was performed
483 using Leica Application Suite X and Image J.

484 Brain tissue was collected from perfusion fixed mice as previously described (59). Animals were
485 anaesthetised with dolethal sodium pentobarbital solution at 125 mg/kg ip (in saline) and transcardially
486 perfused with heparinised 0.1M phosphate buffered saline (1xPBS) followed by 4% PFA in PBS. Brains
487 were extracted and post-fixed in 4% PFA for 24 hrs at 4°C then transferred to 30% sucrose solution at 4°C
488 for 48 hrs. Brains were sectioned coronally from olfactory bulb to the spinomedullary junction at 25 µm
489 using a freezing microtome and stored in cryoprotectant medium. For diaminobenzidine (DAB) staining,
490 antigen retrieval was used for all experiments prior to antibody incubation. Sections were incubated in 10
491 mM sodium citrate (Alfa Aesar, A12274) at 80°C for 10 minutes then washed in PBS. Sections were
492 incubated in 0.5% hydrogen peroxide (Sigma, H1009) in milliQ water for 15 minutes then washed in PBS.
493 Sections were blocked with 5% donkey serum in 0.3% Tween20 (VWR, 437082Q) in PBS (PBST) for 1 hr at
494 room temperature, then incubated with GFP antiserum (1:4000; ab5450, Abcam) in blocking solution
495 overnight at 4°C. After washing in 0.1% PBST, sections were incubated with biotinylated anti-goat IgG
496 (1:400; AP180B, Millipore) in 0.3% PBST for 1.5 hrs at room temperature, followed by a 1 hr incubation
497 with streptavidin conjugated to horseradish peroxidase (Vectastain Elite ABC kit, Vector Laboratories, PK-
498 6100) and developed by DAB substrate (Abcam, ab94665). Sections were washed in PBS, prior to
499 dehydration in ethanol and xylene, then mounting/coverslipping with Pertex mounting medium (Pioneer
500 Research Chemicals Ltd., PRC/R/750). For immunofluorescent staining, slices were washed in PBS, prior
501 to blocking for 1 hr in 5% donkey serum then incubation with primary antisera (table 1) in blocking solution
502 overnight at 4°C. Slices were washed in and incubated with the appropriate secondary antisera (Alexa
503 Fluor® 488 or 555; Invitrogen) diluted 1:500 for 2 hrs at room temperature. Following washing, mounted

504 sections were coverslipped on superfrost slides using Vectashield (Vector Laboratories, H-1400-10). Slides
505 were imaged using an Axio Scan.Z1 slide scanner (Zeiss) and confocal microscope (Leica TCS SP8 X,
506 Wetzlar, Germany) with a 20x or 40x objective as indicated. Images were analysed in Halo Image Analysis
507 Software (Indica Labs) and ImageJ.

Antigen	**Raised In**	**Concentration**	**Source**
GFP	Goat	1:1000 (unless specified)	Abcam, 5450
DSRed (RFP and mCherry)	Rabbit	1:1000	Takara Bio Clontech, 632496
NeuN	Mouse	1:1000	Millipore, MAB377

508 Table 1. Primary antisera used for immunohistochemistry.

509

510 **Dissociation, fluorescence-activated cell sorting (FACS) and single cell RNA sequencing**

511 For hypothalamic samples, single cell suspensions were prepared and pooled from twelve female *Rxfp4-*
512 Cre x EYFP mice (biological replicates) as previously described (59). Briefly, mice were sacrificed by cervical
513 dislocation and the hypothalamus dissected into Hibernate-A medium (ThermoFisher, A1247501)
514 supplemented with 0.25% GlutaMAX (ThermoFisher, 35050061) and 2% B27 (ThermoFisher, A1895601).
515 Tissue was digested in Hibernate-A medium without calcium (BrainBits) containing 20 U/mL Papain
516 (Worthington) and 1% GlutaMAX for 30 min at 37°C under agitation (Thermomixer, 500 rpm). After
517 digestion, tissue was triturated in Hibernate-A medium with 3.5 U/mL DNase I (Sigma, D4263). The
518 trituration supernatant was loaded on top of a BSA gradient prepared in Hibernate-A medium, spun for 5
519 min at 300 rcf, and the pellet was resuspended in Hibernate-A medium + 1% BSA. The cell suspension was
520 filtered through a 70 µm cell strainer into a fresh tube. Fluorescence-activated cell sorting was performed
521 using an Influx Cell Sorter (BD Biosciences, San Jose, CA, USA). Cell gating was set according to cell size
522 (FSC), cell granularity (SSC), FSC pulse-width for singlets, fluorescence at 488 nm/532 nm for EYFP and
523 647/670 nm for nuclear stain with DraQ5 (Biostatus, Shepshed, Leicester, UK) to exclude cellular debris,

524 aggregates and dead cells. Cells were sorted directly into individual wells of 96-well plates containing lysis
525 buffer. 384 YFP-positive cells were isolated and processed using a Smart-Seq2 protocol (60). Libraries
526 were prepared from ~150 pg of DNA using the Nextera XT DNA preparation kit (Illumina, FC-131-1096)
527 and Nextera XT 96-Index kit (Illumina, FC-131-1002). Pooled libraries were run on the Illumina HiSeq 4000
528 at the Cancer Research UK Cambridge Institute Genomics Core. Sequencing reads were trimmed of
529 adapters, aligned to the *Mus musculus* genome (GRCm38, Ensembl annotation version 101) using STAR
530 (v2.7.3a), and raw counts generated using FeatureCounts (Subread v2.0.0). Downstream analyses were
531 performed using the Seurat R package (v4.0.1). Samples were included in the final analyses only if they
532 met all of the following criteria: (a) unique reads > 50%, (b) reads assigned to exons > 20%; (c) number of
533 genes with (FPKM>1) > 3000; (d) total number of unique genes > 200. Genes were included in the final
534 analyses if they were detected in at least 3 samples. Marker genes were identified for clusters using the
535 FindAllMarkers function in the Seurat package; the top 20 gene markers were cross referenced against
536 other bulk and single cell RNAseq databases to assign cell type. Neuronal clusters were identified in a
537 similar fashion using appropriate marker genes.

538

539 **RNAscope**

540 Detection of Mouse *Rxfp4* was performed on fixed, frozen sections using Advanced Cell Diagnostics (ACD)
541 RNAscope® 2.5 LS Reagent Kit-RED (Cat No. 322150), RNAscope® LS 2.5 Probe- Mm-Rxfp4 (Cat No.
542 317588) (ACD, Hayward, CA, USA). To prepare the sections, animals were anaesthetized with sodium
543 pentobarbital solution (50 mg/kg in saline) and transcardially perfused with PBS followed by 4% PFA in
544 PBS. Brains were extracted and post-fixed in 4% PFA for 24 hrs before being transferred to 25% sucrose
545 for 24 hrs at 4°C. Brains were embedded in OCT compound, frozen in a Novec 7000 (Sigma)/dry ice slurry
546 and stored at -80 C. 16µm cryosections containing the hypothalamus were prepared on a Leica CM1950
547 cryostat (Wetzlar, Germany) at -12°C and stored at -20°C until required.

548 Slides were thawed at room temperature for 10 min before baking at 60°C for 45 min. The sections were
549 then post-fixed in pre-chilled 4% PFA for 15 min at 4°C, washed in 3 changes of PBS for 5 min each before
550 dehydration through 50%, 70%, 100% and 100% ethanol for 5 min each. The slides were air-dried for 5
551 min before loading onto a Bond Rx instrument (Leica Biosystems). Slides were prepared using the frozen
552 slide delay prior to pre-treatments using Epitope Retrieval Solution 2 (Cat No. AR9640, Leica Biosystems)
553 at 95°C for 5 min, and ACD Enzyme from the LS Reagent kit at 40°C for 10 minutes. Probe hybridisation
554 and signal amplification were performed according to manufacturer's instructions, with the exception of
555 increased Amp5 incubation time at 30 min. Fast red detection of mouse *Rxfp4* was performed on the Bond
556 Rx using the Bond Polymer Refine Red Detection Kit (Leica Biosystems, Cat No. DS9390) with an incubation
557 time of 20 min. Slides were then removed from the Bond Rx and were heated at 60°C for 1 hr, dipped in
558 xylene and mounted using EcoMount Mounting Medium (Biocare Medical, CA, USA. Cat No. EM897L).
559 Sections were imaged on a Slide Scanner Axio Scan.Z1 microscope (Zeiss) using a 40x air objective. Three
560 z-stack slices spanning 1.5µM were combined into an extended depth of field image (ZEN 2.6, Zeiss). The
561 CZI files were read into Halo Image Analysis Software (Indica Labs).

562

563 **Statistical analysis**

564 Data were plotted using GraphPad Prism 7/8/9 software (GraphPad Software, Inc). Statistical analysis was
565 performed by paired Student's t-tests, one-way ANOVA with multiple comparisons or two-way ANOVA
566 with multiple comparisons, as indicated. N represents biological replicates. Sample size was computed
567 based on pilot data and previously published data. Data are presented as mean ± SEM and probabilities
568 of $p<0.05$ were considered statistically significant in all tests.

569

570

571 **Acknowledgements**

572 Metabolic Research Laboratories support was provided by the following core facilities: Disease Model
573 Core, Genomics and Transcriptomics Core, Histology Core, Imaging Core, and Core Biochemical Assay
574 Laboratory (supported by the MRC [MRC_MC_UU_12012/5] and Wellcome Trust [100574/Z/12/Z]). RNA-
575 sequencing was undertaken at the CRUK Cambridge Institute Genomics Core. Cell sorting was performed
576 at the NIHR Cambridge BRC Cell Phenotyping Hub. We thank the Histopathology/ISH Core Facility at
577 Cancer Research UK- Cambridge Institute, for assistance with *in situ* hybridisation. We also would like to
578 thank Chris Riches and Maša Josipović for initial help with metabolic and operant cages. JAT is supported
579 by a NIHR Clinical Lectureship (CL-2019-14-504). Research in the laboratory of F.M.G. and F.R. is supported
580 by the MRC (MRC_MC_UU_12012/3) and Wellcome Trust (220271/Z/20/Z). O.R.M.W. is supported by a
581 BBSRC iCASE PhD studentship partnered with AstraZeneca. F.M.G. and F.R. act as guarantors for this
582 manuscript.

583

584

585

586 **Author contributions**

587 JEL, ORMW, FMG and FR designed the research studies. JEL, ORMW, DN, CB, LB and AEA conducted
588 experiments. SJK and BG conducted the SmartSeq2 protocol and library preparation for single-cell RNA-
589 sequencing and CAS led the bioinformatic analysis. EC and MT provided the rabies and rAAV viruses for
590 retrograde viral tracing. JAT prepared the tissues and gave guidance for RNAscope. DH and DB co-
591 supervised ORMW and BUP helped with the initial behavioural cage experiments. FR developed the
592 transgenic models. JEL, ORMW, DN, FMG and FR wrote the manuscript. All authors revised and approved
593 the final draft.

594

595 **Competing interests**

F.M.G. is a paid consultant for Kallyope, New York. The Gribble-Reimann lab currently hosts projects that receive funding from AstraZeneca (O.R.M.W., BBSRC-iCASE), Eli Lilly & Company and LGC. DH and DB are AstraZeneca employees and CB and BUP have also joined AstraZeneca since contributing to this work.

References

1. Bathgate RA, Halls ML, van der Westhuizen ET, Callander GE, Kocan M, Summers RJ. Relaxin family peptides and their receptors. Physiol Rev. 2013;93(1):405-80.
2. Ang SY, Hutchinson DS, Evans BA, Hossain MA, Patil N, Bathgate RA, et al. The actions of relaxin family peptides on signal transduction pathways activated by the relaxin family peptide receptor RXFP4. Naunyn Schmiedebergs Arch Pharmacol. 2017;390(1):105-11.
3. Liu C, Lovenberg TW. Relaxin-3, INSL5, and their receptors. Results Probl Cell Differ. 2008;46:213-37.
4. Grosse J, Heffron H, Burling K, Akhter Hossain M, Habib AM, Rogers GJ, et al. Insulin-like peptide 5 is an orexigenic gastrointestinal hormone. Proceedings of the National Academy of Sciences of the United States of America. 2014;111(30):11133-8.
5. Lewis JE, Miedzybrodzka EL, Foreman RE, Woodward ORM, Kay RG, Goldspink DA, et al. Selective stimulation of colonic L cells improves metabolic outcomes in mice. Diabetologia. 2020;63(7):1396-407.
6. Billing LJ, Smith CA, Larraufie P, Goldspink DA, Galvin S, Kay RG, et al. Co-storage and release of insulin-like peptide-5, glucagon-like peptide-1 and peptideYY from murine and human colonic enteroendocrine cells. Mol Metab. 2018.
7. Lee YS, De Vadder F, Tremaroli V, Wichmann A, Mithieux G, Bäckhed F. Insulin-like peptide 5 is a microbially regulated peptide that promotes hepatic glucose production. Mol Metab. 2016;5(4):263-70.
8. Zaykov AN, Gelfanov VM, Perez-Tilve D, Finan B, DiMarchi RD. Insulin-like peptide 5 fails to improve metabolism or body weight in obese mice. Peptides. 2019;120:170116.
9. Liu C, Kuei C, Sutton S, Chen J, Bonaventure P, Wu J, et al. INSL5 is a high affinity specific agonist for GPCR142 (GPR100). J Biol Chem. 2005;280(1):292-300.
10. Boels K, Schaller HC. Identification and characterisation of GPR100 as a novel human G-protein-coupled bradykinin receptor. Br J Pharmacol. 2003;140(5):932-8.
11. Liu C, Chen J, Sutton S, Roland B, Kuei C, Farmer N, et al. Identification of relaxin-3/INSL7 as a ligand for GPCR142. J Biol Chem. 2003;278(50):50765-70.
12. Musatov S, Chen W, Pfaff DW, Mobbs CV, Yang XJ, Clegg DJ, et al. Silencing of estrogen receptor alpha in the ventromedial nucleus of hypothalamus leads to metabolic syndrome. Proc Natl Acad Sci U S A. 2007;104(7):2501-6.
13. Luo SX, Huang J, Li Q, Mohammad H, Lee CY, Krishna K, et al. Regulation of feeding by somatostatin neurons in the tuberal nucleus. Science. 2018;361(6397):76-81.
14. Muntean BS, Zucca S, MacMullen CM, Dao MT, Johnston C, Iwamoto H, et al. Interrogating the Spatiotemporal Landscape of Neuromodulatory GPCR Signaling by Real-Time Imaging of cAMP in Intact Neurons and Circuits. Cell Rep. 2018;22(1):255-68.
15. Kim DW, Yao Z, Graybuck LT, Kim TK, Nguyen TN, Smith KA, et al. Multimodal Analysis of Cell Types in a Hypothalamic Node Controlling Social Behavior. Cell. 2019;179(3):713-28.e17.

636 16. van Veen JE, Kammel LG, Bunda PC, Shum M, Reid MS, Massa MG, et al. Hypothalamic estrogen
637 receptor alpha establishes a sexually dimorphic regulatory node of energy expenditure. Nat Metab.
638 2020;2(4):351-63.
639 17. Li MM, Madara JC, Steger JS, Krashes MJ, Balthasar N, Campbell JN, et al. The Paraventricular
640 Hypothalamus Regulates Satiety and Prevents Obesity via Two Genetically Distinct Circuits. Neuron.
641 2019;102(3):653-67.e6.
642 18. Wall NR, Wickersham IR, Cetin A, De La Parra M, Callaway EM. Monosynaptic circuit tracing in
643 vivo through Cre-dependent targeting and complementation of modified rabies virus. Proc Natl Acad Sci
644 U S A. 2010;107(50):21848-53.
645 19. Jendryka M, Palchaudhuri M, Ursu D, van der Veen B, Liss B, Kätzel D, et al. Pharmacokinetic and
646 pharmacodynamic actions of clozapine-N-oxide, clozapine, and compound 21 in DREADD-based
647 chemogenetics in mice. Sci Rep. 2019;9(1):4522.
648 20. Woodward ORM, Gribble FM, Reimann F, Lewis JE. Gut peptide regulation of food intake -
649 evidence for the modulation of hedonic feeding. The Journal of physiology. 2021.
650 21. Mashima H, Ohno H, Yamada Y, Sakai T, Ohnishi H. INSL5 may be a unique marker of colorectal
651 endocrine cells and neuroendocrine tumors. Biochem Biophys Res Commun. 2013;432(4):586-92.
652 22. Thanasupawat T, Hammje K, Adham I, Ghia JE, Del Bigio MR, Krcek J, et al. INSL5 is a novel marker
653 for human enteroendocrine cells of the large intestine and neuroendocrine tumours. Oncol Rep.
654 2013;29(1):149-54.
655 23. Ebling FJP, Lewis JE. Tanycytes and hypothalamic control of energy metabolism. Glia.
656 2018;66(6):1176-84.
657 24. Rogge G, Jones D, Hubert GW, Lin Y, Kuhar MJ. CART peptides: regulators of body weight, reward
658 and other functions. Nat Rev Neurosci. 2008;9(10):747-58.
659 25. Cavuoto P, Wittert GA. The role of the endocannabinoid system in the regulation of energy
660 expenditure. Best Pract Res Clin Endocrinol Metab. 2009;23(1):79-86.
661 26. Xu B, Goulding EH, Zang K, Cepoi D, Cone RD, Jones KR, et al. Brain-derived neurotrophic factor
662 regulates energy balance downstream of melanocortin-4 receptor. Nat Neurosci. 2003;6(7):736-42.
663 27. Sampson CM, Kasper JM, Felsing DE, Raval SR, Ye N, Wang P, et al. Small-Molecule Neuromedin
664 U Receptor 2 Agonists Suppress Food Intake and Decrease Visceral Fat in Animal Models. Pharmacol Res
665 Perspect. 2018;6(5):e00425.
666 28. Moon YS, Smas CM, Lee K, Villena JA, Kim KH, Yun EJ, et al. Mice lacking paternally expressed Pref-
667 1/Dlk1 display growth retardation and accelerated adiposity. Mol Cell Biol. 2002;22(15):5585-92.
668 29. Wermter AK, Scherag A, Meyre D, Reichwald K, Durand E, Nguyen TT, et al. Preferential reciprocal
669 transfer of paternal/maternal DLK1 alleles to obese children: first evidence of polar overdominance in
670 humans. Eur J Hum Genet. 2008;16(9):1126-34.
671 30. Viskaitis P, Irvine EE, Smith MA, Choudhury AI, Alvarez-Curto E, Glegola JA, et al. Modulation of
672 SF1 Neuron Activity Coordinately Regulates Both Feeding Behavior and Associated Emotional States. Cell
673 Rep. 2017;21(12):3559-72.
674 31. Wang D, He X, Zhao Z, Feng Q, Lin R, Sun Y, et al. Whole-brain mapping of the direct inputs and
675 axonal projections of POMC and AgRP neurons. Front Neuroanat. 2015;9:40.
676 32. Williams G, Bing C, Cai XJ, Harrold JA, King PJ, Liu XH. The hypothalamus and the control of energy
677 homeostasis: different circuits, different purposes. Physiology & behavior. 2001;74(4-5):683-701.
678 33. Kelley AE, Baldo BA, Pratt WE, Will MJ. Corticostriatal-hypothalamic circuitry and food motivation:
679 integration of energy, action and reward. Physiology & behavior. 2005;86(5):773-95.
680 34. Kenny PJ. Reward mechanisms in obesity: new insights and future directions. Neuron.
681 2011;69(4):664-79.
682 35. Tobiansky DJ, Roma PG, Hattori T, Will RG, Nutsch VL, Dominguez JM. The medial preoptic area
683 modulates cocaine-induced activity in female rats. Behav Neurosci. 2013;127(2):293-302.

684 36. Tryon VL, Mizumori SJY. A Novel Role for the Periaqueductal Gray in Consummatory Behavior.
685 Front Behav Neurosci. 2018;12:178.
686 37. Wu Q, Boyle MP, Palmiter RD. Loss of GABAergic signaling by AgRP neurons to the parabrachial
687 nucleus leads to starvation. Cell. 2009;137(7):1225-34.
688 38. Chiang MC, Bowen A, Schier LA, Tupone D, Uddin O, Heinricher MM. Parabrachial Complex: A Hub
689 for Pain and Aversion. J Neurosci. 2019;39(42):8225-30.
690 39. Lo L, Yao S, Kim DW, Cetin A, Harris J, Zeng H, et al. Connectional architecture of a mouse
691 hypothalamic circuit node controlling social behavior. Proc Natl Acad Sci U S A. 2019;116(15):7503-12.
692 40. King BM. The rise, fall, and resurrection of the ventromedial hypothalamus in the regulation of
693 feeding behavior and body weight. Physiol Behav. 2006;87(2):221-44.
694 41. MILLER NE, BAILEY CJ, STEVENSON JA. Decreased "hunger" but increased food intake resulting
695 from hypothalamic lesions. Science. 1950;112(2905):256-9.
696 42. TEITELBAUM P. Random and food-directed activity in hyperphagic and normal rats. J Comp Physiol
697 Psychol. 1957;50(5):486-90.
698 43. Grossman SP. The

699 VMH: a center for affective reactions, satiety, or both? . 1966;1:1-10.
700 44. Lindberg D, Chen P, Li C. Conditional viral tracing reveals that steroidogenic factor 1-positive
701 neurons of the dorsomedial subdivision of the ventromedial hypothalamus project to autonomic centers
702 of the hypothalamus and hindbrain. J Comp Neurol. 2013;521(14):3167-90.
703 45. Hashikawa K, Hashikawa Y, Tremblay R, Zhang J, Feng JE, Sabol A, et al. Esr1. Nat Neurosci.
704 2017;20(11):1580-90.
705 46. Coutinho EA, Okamoto S, Ishikawa AW, Yokota S, Wada N, Hirabayashi T, et al. Activation of SF1
706 Neurons in the Ventromedial Hypothalamus by DREADD Technology Increases Insulin Sensitivity in
707 Peripheral Tissues. Diabetes. 2017;66(9):2372-86.
708 47. Yang CF, Chiang MC, Gray DC, Prabhakaran M, Alvarado M, Juntti SA, et al. Sexually dimorphic
709 neurons in the ventromedial hypothalamus govern mating in both sexes and aggression in males. Cell.
710 2013;153(4):896-909.
711 48. Lee H, Kim DW, Remedios R, Anthony TE, Chang A, Madisen L, et al. Scalable control of mounting
712 and attack by Esr1+ neurons in the ventromedial hypothalamus. Nature. 2014;509(7502):627-32.
713 49. Krause WC, Ingraham HA. Origins and Functions of the Ventrolateral VMH: A Complex Neuronal
714 Cluster Orchestrating Sex Differences in Metabolism and Behavior. Adv Exp Med Biol. 2017;1043:199-213.
715 50. Correa SM, Newstrom DW, Warne JP, Flandin P, Cheung CC, Lin-Moore AT, et al. An estrogen-
716 responsive module in the ventromedial hypothalamus selectively drives sex-specific activity in females.
717 Cell Rep. 2015;10(1):62-74.
718 51. Ma S, Smith CM, Blasiak A, Gundlach AL. Distribution, physiology and pharmacology of relaxin-
719 3/RXFP3 systems in brain. Br J Pharmacol. 2017;174(10):1034-48.
720 52. Atasoy D, Aponte Y, Su HH, Sternson SM. A FLEX switch targets Channelrhodopsin-2 to multiple
721 cell types for imaging and long-range circuit mapping. J Neurosci. 2008;28(28):7025-30.
722 53. Shimshek DR, Kim J, Hübner MR, Spergel DJ, Buchholz F, Casanova E, et al. Codon-improved Cre
723 recombinase (iCre) expression in the mouse. Genesis. 2002;32(1):19-26.
724 54. Srinivas S, Watanabe T, Lin CS, William CM, Tanabe Y, Jessell TM, et al. Cre reporter strains
725 produced by targeted insertion of EYFP and ECFP into the ROSA26 locus. BMC Dev Biol. 2001;1:4.
726 55. Zhu H, Aryal DK, Olsen RH, Urban DJ, Swearingen A, Forbes S, et al. Cre-dependent DREADD
727 (Designer Receptors Exclusively Activated by Designer Drugs) mice. Genesis. 2016;54(8):439-46.
728 56. Zariwala HA, Borghuis BG, Hoogland TM, Madisen L, Tian L, De Zeeuw CI, et al. A Cre-dependent
729 GCaMP3 reporter mouse for neuronal imaging in vivo. J Neurosci. 2012;32(9):3131-41.

730 57. Luche H, Weber O, Nageswara Rao T, Blum C, Fehling HJ. Faithful activation of an extra-bright red
731 fluorescent protein in "knock-in" Cre-reporter mice ideally suited for lineage tracing studies. Eur J
732 Immunol. 2007;37(1):43-53.
733 58. Heath CJ, Phillips BU, Bussey TJ, Saksida LM. Measuring Motivation and Reward-Related Decision
734 Making in the Rodent Operant Touchscreen System. Current protocols in neuroscience. 2016;74:8.34.1-
735 8..20.
736 59. Adriaenssens AE, Biggs EK, Darwish T, Tadross J, Sukthankar T, Girish M, et al. Glucose-Dependent
737 Insulinotropic Polypeptide Receptor-Expressing Cells in the Hypothalamus Regulate Food Intake. Cell
738 metabolism. 2019;30(5):987-96.e6.
739 60. Picelli S, Björklund Å, Faridani OR, Sagasser S, Winberg G, Sandberg R. Smart-seq2 for sensitive
740 full-length transcriptome profiling in single cells. Nat Methods. 2013;10(11):1096-8.

741

742

743 **Figure Legends**

744 **Figure 1: RXFP4 is expressed in the central nervous system.**

745 a) Scaled schematic of the bacterial artificial chromosome used to make *Rxfp4*-Cre mice. b) Crossing of
746 *Rxfp4*-Cre mice with GFP-based reporter mice (EYFP or GCaMP3) used to detect *Rxfp4* expression in Fig 1
747 through GFP immunohistochemistry. c) Representative section from the colon of RXFP4^{EYFP} mice
748 demonstrating *Rxfp4* expression in epithelial cells. Scale bar = 100 μm. d,e) Coronal section of RXFP4^{GCaMP3}
749 mice showing distinct *Rxfp4*-expressing cell clusters in the ventrolateral part of the ventromedial
750 hypothalamus (VMHvl) and adjacent central VMH (VMHc) tuberal nucleus (TN). Scale bars = 500 μm. f)
751 Co-staining for DAPI (blue), GFP (green) and NeuN (red) in the VMH of RXFP4^{GCaMP3} mice. Scale bar = 100
752 μm. g,h) Coronal sections of C57Bl6 mice labelled for *Rxfp4* mRNA in the VMH using RNAscope. Scale bar
753 = 1 mm and 50 μm in the enlarged image (h). i)Representative trace of a recorded cell in a RXFP4^{CAMPER}
754 slice responding to IBMX (100uM) in the absence and presence of INSL5 (100nM) and Forskolin (10uM),
755 as indicated. 14 out of 54 cells responded to INSL5 with the same pattern (n=5 mice). j, k, l) Food intake
756 of wildtype mice following intra-VMH infusion of vehicle/INSL5 (5 μg) (standard chow t=1.081, p = 0.3008
757 n=13, HFD (45%) t=3.529 n=6, p = 0.0168, liquid Ensure (HPM) t = 3.902, p = 0.0114 n=6, paired two-tailed
758 t test, animals adapted to the appearance of test meal over the course of two weeks prior to surgery and
759 recovery, testing conducted between 12:00-15:00).

760 **Suppl. Fig 1: *Rxfp4* expression in the central nervous system**

761 Coronal sections from RXFP4^{GCaMP3} mice stained for GFP immunoreactivity reveal *Rxfp4* expression in
762 various central nuclei. Red circles represent the presence of immunoreactive cells. Reference images
763 based on the Paxinos Mouse Brain Atlas with the A/P coordinates from bregma indicated in the top left
764 corner. AOB: Accesory olfactory bulb; GrO: Granular cell layer of the olfactory; vn: vomeronasal nerve;
765 ACC: anterior cingulate cortex; SSC: somatosensory cortex; GI: granular insular cortex; SFi: septofimbrial
766 nucleus; TS: triangular septal nucleus; SFO: subfornical organ; NBD: nucleus of the diagonal band; AV:

767 anteroventral thalamic nucleus; AHA: anterior hypothalamic area; PLH: peduncular lateral hypothalamus;
768 PVH: paraventricular hypothalamus; MCPO: magnocellular preoptic nucleus; AA: anterior amygdaloid
769 area; SI: substantia innominata; GP: globus pallidus; RSC: retrosplenial cortex; MHb: medial habenular
770 nucleus; CeA: central amygdala; CoA: cortical amygdala; DEn: dorsal endopiriform nucleus; DMH:
771 dorsomedial hypothalamus; VMHvl: ventromedial hypothalamus ventrolateral part; ARC: arcuate nucleus;
772 ZI: zona incerta; BLA: basolateral amygdala; DS: dorsal subiculum; SC: superior colliculus; PAG:
773 periaqueductal grey (D: dorsal, L: lateral, VL: ventrolateral); scp: superior cerebellar peduncle; SuM:
774 supramammillary nucleus; MM: medial mammillary nucleus; MnM: medial mammillary nucleus median
775 part; LM: lateral mammillary nucleus; PMCoA: posteromedial cortical amydala; PnO: pontine reticular
776 nucleus oral part; ml: medial lemniscus; lfp: longitudinal fasciculus of the pons; Cu: cuneate nucleus; Sp5:
777 spinal trigeminal tract (C: caudal part, I: interpolar part).

778 **Figure 2: Transcriptomic profiling of hypothalamic *Rxfp4*-expressing cells by scRNAseq**

779 a,b) tSNE visualisation of 350 hypothalamic *Rxfp4*-expressing cells indicates five clusters (a). Cell types
780 were assigned according to the expression of a combination of canonical cell-type markers genes (b). The
781 red circle indicates the neuronal cluster used in further analysis. c) tSNE visualisation of the 95 neuronal
782 cells revealed 7 sub-clusters. D) Violin plots showing expression of marker genes associated with multiple
783 neuronal cell types. All gene expression counts are log-normalised with scale-factor = 10^4.

784 **Suppl. Fig 2: Transcriptomic profiling of the neuronal cluster from scRNAseq of hypothalamic *Rxfp4*-**
785 **expressing cells**

786 Violin plots showing expression of multiple genes in the hypothalamic *Rxfp4*-expressing neuronal sub-
787 clusters. All gene expression counts are log-normalised with scale-factor = 10^4.

788 **Figure 3: Circuit mapping of hypothalamic *Rxfp4*-expressing cells**

789 a) Schematic illustrating unilateral microinjection of rAAV8-DIO-hChR2(H134R)-mCherry into the
790 VMH of RXFP4^{GCaMP3} mice. B) Immunofluorescence images demonstrating co-localisation of GFP

791 (green) and ChR2-mCherry (red) starter cells in the target region at A/P -1.7mm from bregma. C)
792 Representative images showing ChR2-mCherry-immunoreactive axon terminals in various brain
793 regions (n=3). For each image, distance from bregma (in mm) is indicated at the bottom right.
794 Scale bars = 100 µm. 40x magnification. D) Schematic illustrating unilateral microinjection of
795 AVV2-TVAeGFP-oG into the VMH of *Rxfp4*-Cre mice followed by a unilateral microinjection of Rab-
796 ΔG-EnvA-mCherry 21 days later. E) Immunofluorescence images demonstrating the colocalisation
797 of GFP (green) and Rab-mCherry (red) starter cells in the target region A/P -1.7mm from bregma.
798 F) Representative immunofluorescence images showing Rab-mCherry-immunoreactive cell
799 bodies in various brain regions (n=3). For each image distance from bregma (in mm) is indicated
800 at the bottom right. 20x magnification. G) Schematic illustrating the regions positive for
801 anterograde projections (red arrows), retrograde projections (blue arrows) or bilateral
802 projections (black arrows) from RXFP4^{VMH} cells. Abbreviations: ARC: arcuate nucleus; BNST: bed
803 nucleus of the stria terminalis; CeA: central amygdala; LHA: lateral hypothalamic area; PAG:
804 periaqueductal grey; PMN: premammillary nucleus; POA: Preoptic area; PVH: paraventricular
805 hypothalamus; PVT: paraventricular thalamic nucleus; VMH: ventromedial hypothalamus.

806 **Suppl. Fig 3: Anterograde projection regions from RXFP4^{VMH} cells**

807 Representative images showing ChR2-mCherry-immunoreactive axon terminals in other brain regions,
808 further to those already indicated in Fig 6 (n=3). For each image, distance from bregma (in mm) is indicated
809 at the bottom right. Scale bars = 100 µm. 40x magnification. Abbreviations: AHA: anterior hypothalamic
810 area; ARC: arcuate nucleus; DMH: dorsomedial hypothalamus; EAC: extended amygdala central part; LC:
811 locus coeruleus; LHA: lateral hypothalamic area; LPBN: lateral parabrachial nucleus; MPBN: medial
812 parabrachial nucleus; PMNd: premammillary nucleus dorsal part; SI: substantia innominata; SuM:
813 supramammillary nucleus; VTA: ventral tegmental area.

814 **Figure 4: VMH ablation of RXFP4 expressing cells regulates food intake and body weight.**

815 a) rAAV-mCherry (control) or rAAV-DTA were bilaterally injected into the ventromedial
816 hypothalamus of *Rxfp4*^{GCaMP3} mice. B) Targeting efficiency was confirmed post perfusion fixation
817 by GFP-immunohistochemistry. Representative images showing efficient ablation in the VMH. C)
818 Body weight following exposure to standard chow and HFD in parallel (effect of time [F(1.423,
819 22.76) = 44.45, p < 0.0001], effect of treatment [F(1,16) = 5.687, p = 0.03) (n = 8-10 per group). D)
820 RER effect of time [F(6.263, 87.69) = 3.368, p = 0.0044)], effect of treatment [F(1, 14) = 6.669, p =
821 0.02]. E) Energy expenditure effect of time [F(9.339,130.7) = 20.34, p < 0.0001], effect of
822 treatment [F(1,14) = 0.004, p = 0.95] and f) ambulatory activity effect of time [F(7.723, 100.4) =
823 11.69, p < 0.0001], effect of treatment [F(1,16) = 3.270, p = 0.09] of mice housed in metabolic
824 cages 5 weeks post-surgery. G) Average 24hr food intake (effect of diet [F(2,42) = 61.97, p <
825 0.0001) and effect of treatment [F(1.42) = 28.27, p < 0.0001) h) Average 24hr meal duration (effect
826 of diet [F(1,28) = 0.02361, p = 0.88) and effect of treatment [F(1,28) = 1.393, p = 0.25) and i)
827 Average 24hr interval between meals (effect of diet [F(1,28) = 10.08, p = 0.0046) and effect of
828 treatment [F(1,28) = 21.71, p < 0.0001) of mice treated with rAAV-mCherry or rAAV-DTA of
829 RXFP4^{VMHKO} mice in metabolic chambers, when mice had access to a choice between std chow and
830 a HFD (rAAV-mCherry n = 6, rAAV-DTA n =10 respectively, group mean ± SEM).

831 **Figure 5: CNO alters feeding and food preference in RXFP4$^{wb\text{-}Di}$ mice.**

832 a) Schematic of RXFP4$^{wb\text{-}Di}$ mouse model. b-d) Food intake in RXFP4$^{wb\text{-}Di}$ mice of standard chow
833 (t=0.5536, p = 0.5875) (b) or HFD (45%) (t=2.612, p = 0.019) (c) or liquid Ensure (HPM) (t=2.648, p
834 = 0018) (d) 1 hour post CNO/vehicle treatment at 11:00 (n = 17, paired two-tailed t test, animals
835 adapted to the appearance of test meal over the course of two weeks). (e) 1st hr (effect of
836 treatment [F(1,36)=14.86, p = 0.0005], std chow p = 0.7604, HFD p = 0.03, kcal p = 0.012) and (f)
837 2nd hr food (effect of treatment [F(1,36)=2.219, p = 0.15], std chow p = 0.9918, HFD p = 0.6691,

838 kcal p = 0.50) consumption after CNO (orange) or saline (black) injection at 11:00 in mice housed
839 in metabolic chambers (n = 7 , two-way ANOVA with Sidak's multiple-comparison test) when mice
840 had a choice between std chow or HFD.

841 **Figure 6: CNO alters feeding and food preference in RXFP4$^{wb\text{-}Dq}$ mice**

842 a) Schematic of RXFP4$^{wb\text{-}Dq}$ mouse model. b-d) Food intake of (b) standard chow (t=0.1.235, p = 0.2628) (c)
843 HFD (45%) (t=5.136, p = 0.0021) and (d) liquid Ensure (HPM) (t=7.725, p = 0.0002) 1 hour post CNO/saline
844 treatment at 19:00 (n = 7, paired two-tailed t test, animals adapted to the appearance of test meal over
845 the course of two weeks). e) 1st hr (effect of treatment [F(1,42) = 13.17, p = 0.0008, standard chow p =
846 0.9321, HFD p = 0.0377, kcal p = 0.009) and f) 2nd hr (effect of treatment [F(1,36)=0.1177, p = 0.7335], std
847 chow p = 0.9475, HFD p = 0.8197, kcal p = 0.9875) food consumption after CNO (orange) or saline (black)
848 injection at 19:00 in mice housed in metabolic chambers (n = 7, two-way ANOVA with Sidak's multiple-
849 comparison test) when mice had access to a choice between std chow and a HFD. g-i) Performance
850 parameters in mice trained in operant chambers when treated with CNO (orange) or vehicle (black): g)
851 Number of rewards earned in FR5 (n = 12, t=6.874, p < 0.001, paired two-tailed t test). h) Breakpoint in
852 PR4 (number of target responses emitted by an animal in the last successfully completed trial, before
853 session termination or 60 min time-out) (n = 12, t=9.357, *** p < 0.001, paired two tailed t test). i) ERC
854 performance post vehicle (black) or CNO (orange) treatment between 11-13:00 (n = 12, effect of
855 treatment [F(1,44)=41.38, p < 0.0001, std chow p = 0.72, HPM p < 0.0001, two-way ANOVA with Sidak's
856 multiple-comparison test, animals calorically restricted to 95% BW).

857 **Figure 7: Ventromedial hypothalamic *Rxfp4*-expressing neurons regulate food preference.**

858 a) rAAV-hM3Dq-mCherry was bilaterally injected into the ventromedial hypothalamus of *Rxfp4*-Cre mice.
859 b) Targeting efficiency was confirmed post perfusion fixation. Representative image showing ARC, DMH,
860 VMH and TN with only VMH demonstrating rAAV-hM3Dq-mCherry expression. c) Representative images

861 of RXFP4^{VMHDq} cells before, during and after bath applied CNO (15 µM) showing somatic GCaMP3
862 fluorescence (top panel), with traces from individual cells (bottom panel, mean intensity shown in red).
863 d) Quantification of responses showing median AUC before and during bath applied CNO (t= 3.285, p =
864 0.0047 paired two-tailed t test, n = 17 cells from 3 mice). e-f) Food intake of (e) standard chow (t=0.63, p
865 = 0.5371) (f) HFD (45%) (t=5.630, p < 0.0001) and (g) liquid Ensure (HPM) (t=3.714, 0.0017) 1 hour post
866 CNO (orange) or vehicle (black) treatment at 19:00 (n = 18, paired two-tailed t test, animals adapted to
867 the appearance of test meal over the course of two weeks. (h) 1st hr (effect of treatment [F(1,98)=14.70,
868 p = 0.0002, std chow p > 0.9999, HFD p = 0.003, kcal p = 0.0067) and (i) 2nd hr (effect of treatment
869 [F(1,102)=1.65, p = 0.2014, std chow p = 0.9552, HFD p = 0.887, kcal p = 0.6080) food consumption of
870 RXFP4^{VMHDq} mice in metabolic chambers, when mice had access to a choice between std chow and a HFD,
871 post CNO (orange) or vehicle (black) treatment (n = 18 per group, mean ± SEM). Scale bars = 100µm.

872 **Suppl. Fig 4: Calorimetric data from RXFP4 Di and Dq mice**

873 Ambulatory activity (a,c,e) and energy expenditure (b,d,f) of RXFP4$^{wb\text{-}Di}$ (a,b, effect of time [F(8.262, 115.7)
874 = 2.092, p = 0.0402] and effect of time [F(11.52, 161.3) = 8.018, p < 0.0001] respectively), RXFP4$^{wb\text{-}Dq}$ (c,d,
875 effect of time [F(3.934,55.08) = 1.610, p = 0.0137 and effect of treatment [F(1, 13) = 5.860, p = 0.0309)
876 and RXFP4^{VMHDq} (e,f, effect of time [F(288, 4018) = 3.622, p < 0.0001) and effect of time [F(4.194, 58.01) =
877 4.400, p = 0.0031) mice housed in metabolic cages in response to CNO (orange) or saline (black).
878 Conditions and stats as in Fig 2 (Di), Fig 3 (Dq) and Fig 5 (VMH-Dq), respectively.

879

880

881

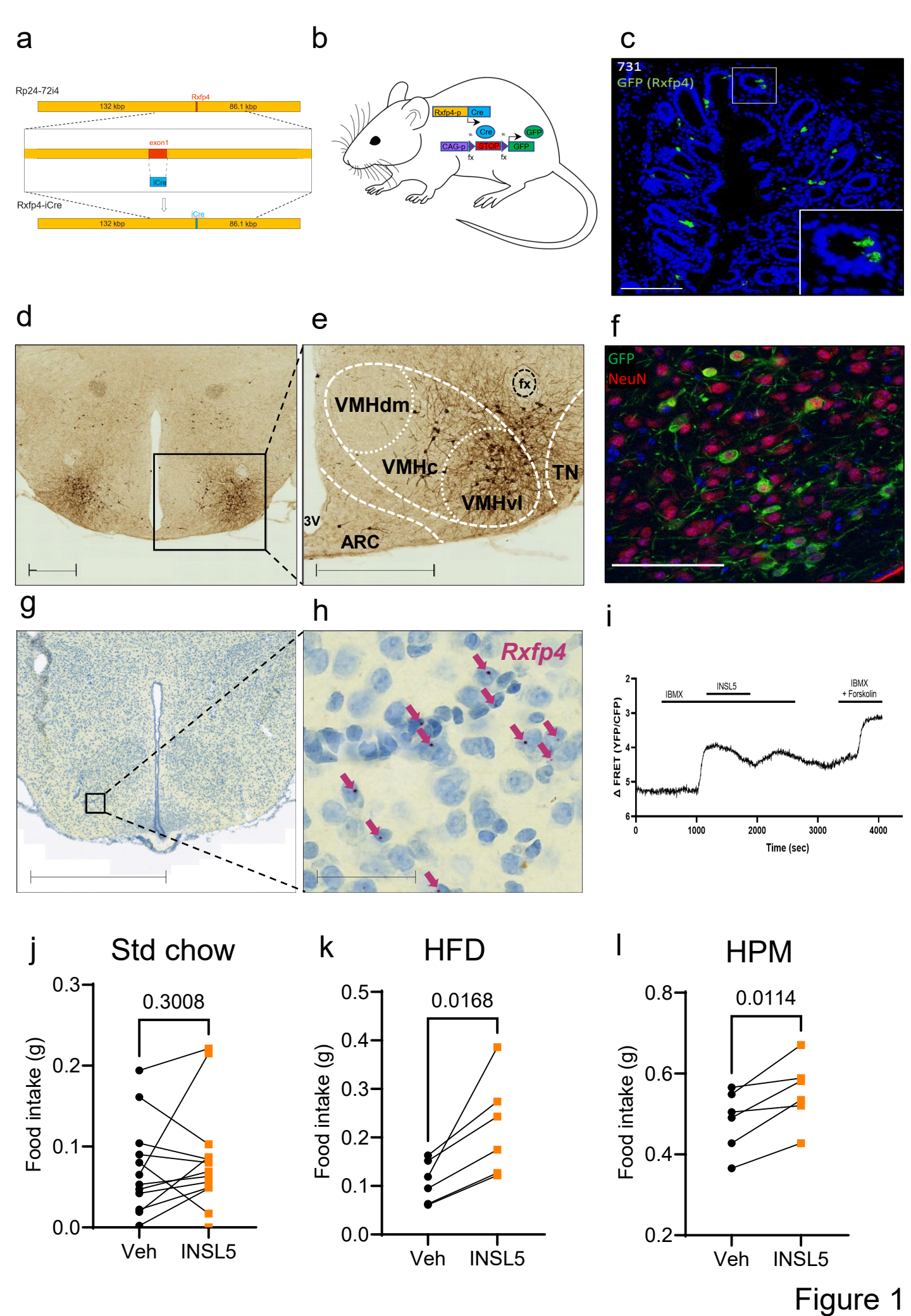
a
Rp24-72i4
Rxfp4
132 kbp
86.1 kbp
exon1
iCre
Rxfp4-iCre
iCre
132 kbp
86.1 kbp
b
Rxfp4-p
Cre
Cre
GFP
CAG-p
STOP
GFP
fx
fx
c
731
GFP (Rxfp4)
d
e
VMHdm
fx
VMHc
TN
VMHvl
3V
ARC
f
GFP
NeuN
g
h
Rxfp4
i
IBMX
INSL5
IBMX
+ Forskolin
Δ FRET (YFP/CFP)
Time (sec)
j
Std chow
0.3008
Food intake (g)
Veh
INSL5
k
HFD
0.0168
Food intake (g)
Veh
INSL5
l
HPM
0.0114
Food intake (g)
Veh
INSL5

Figure 1

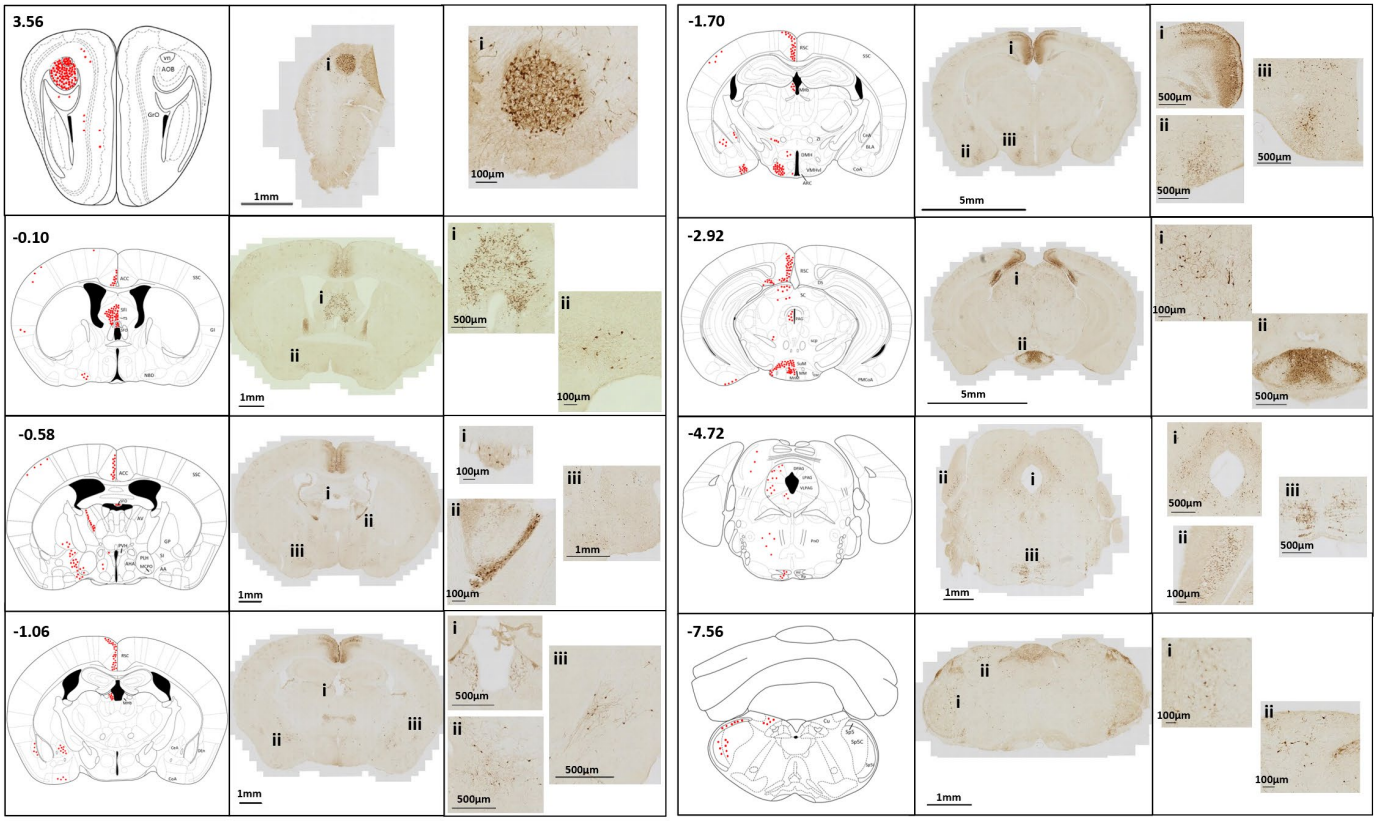

Supplementary Figure 1

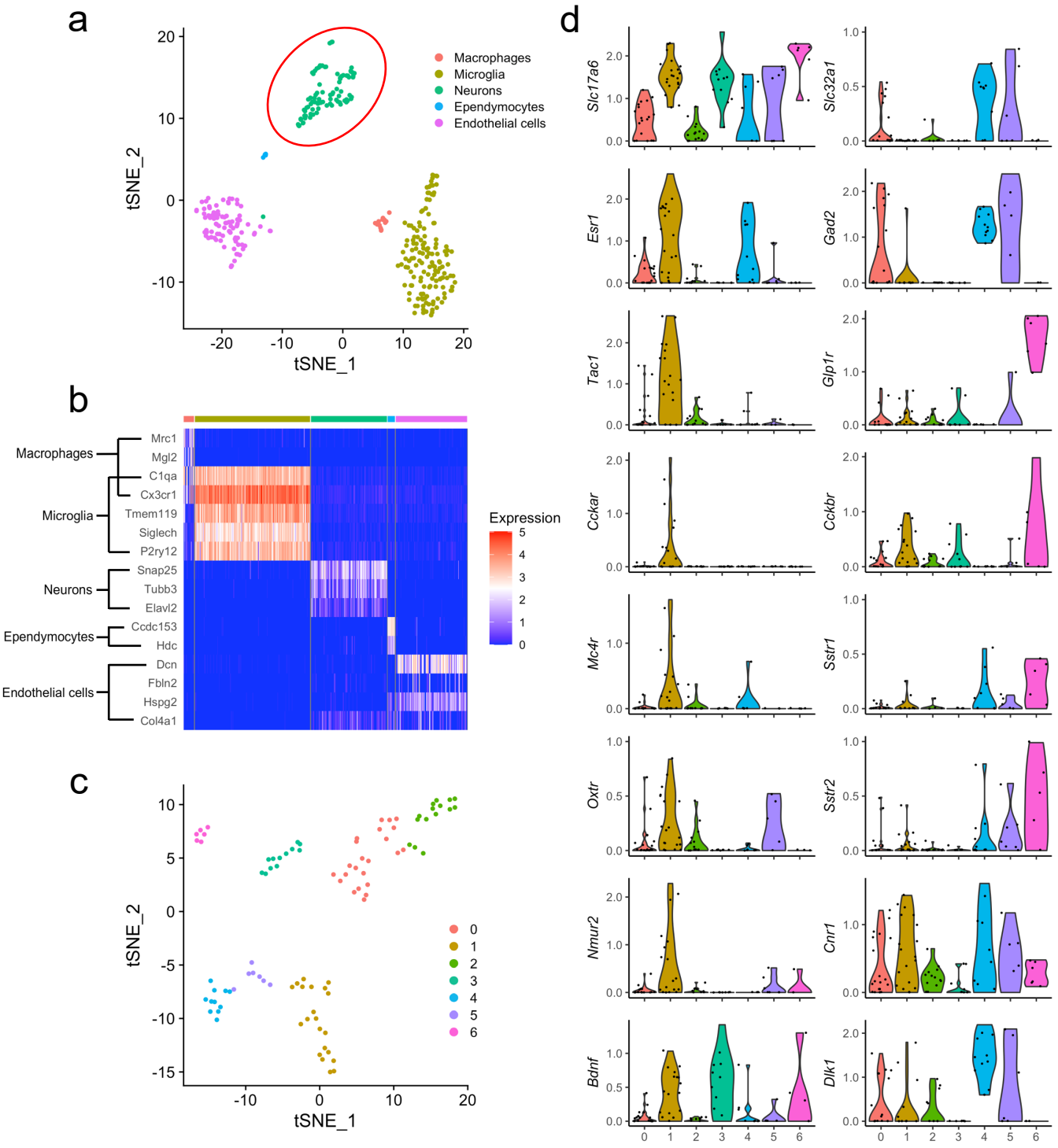
a
Macrophages
Microglia
Neurons
Ependymocytes
Endothelial cells
tSNE_2
tSNE_1
b
Macrophages
Microglia
Neurons
Ependymocytes
Endothelial cells
Mrc1
Mgl2
C1qa
Cx3cr1
Tmem119
Siglech
P2ry12
Snap25
Tubb3
Elavl2
Ccdc153
Hdc
Dcn
Fbln2
Hspg2
Col4a1
Expression
c
tSNE_2
tSNE_1
d
Slc17a6
Slc32a1
Esr1
Gad2
Tac1
Glp1r
Cckar
Cckbr
Mc4r
Sstr1
Oxtr
Sstr2
Nmur2
Cnr1
Bdnf
Dlk1

Figure 2

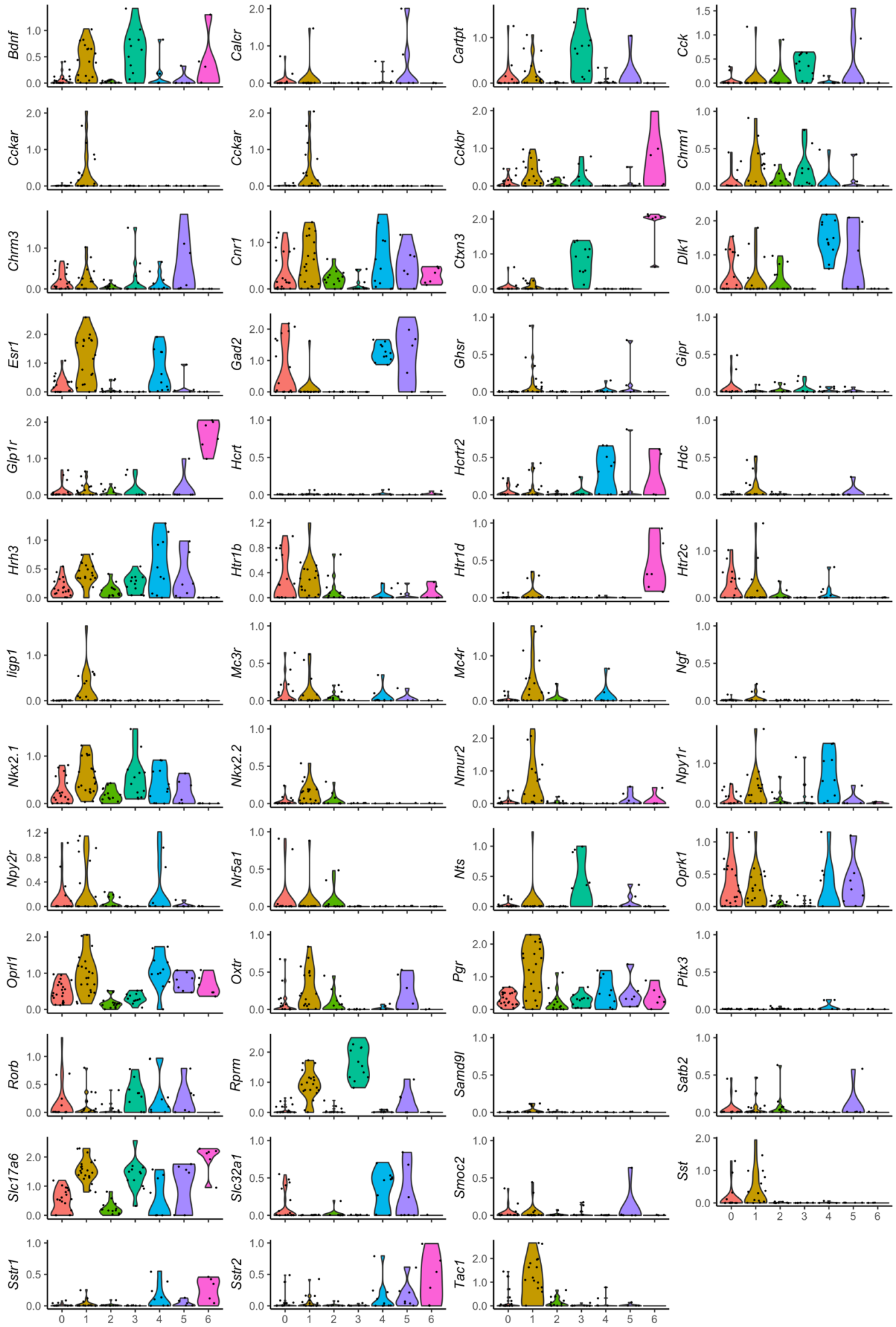

Supplementary figure 2

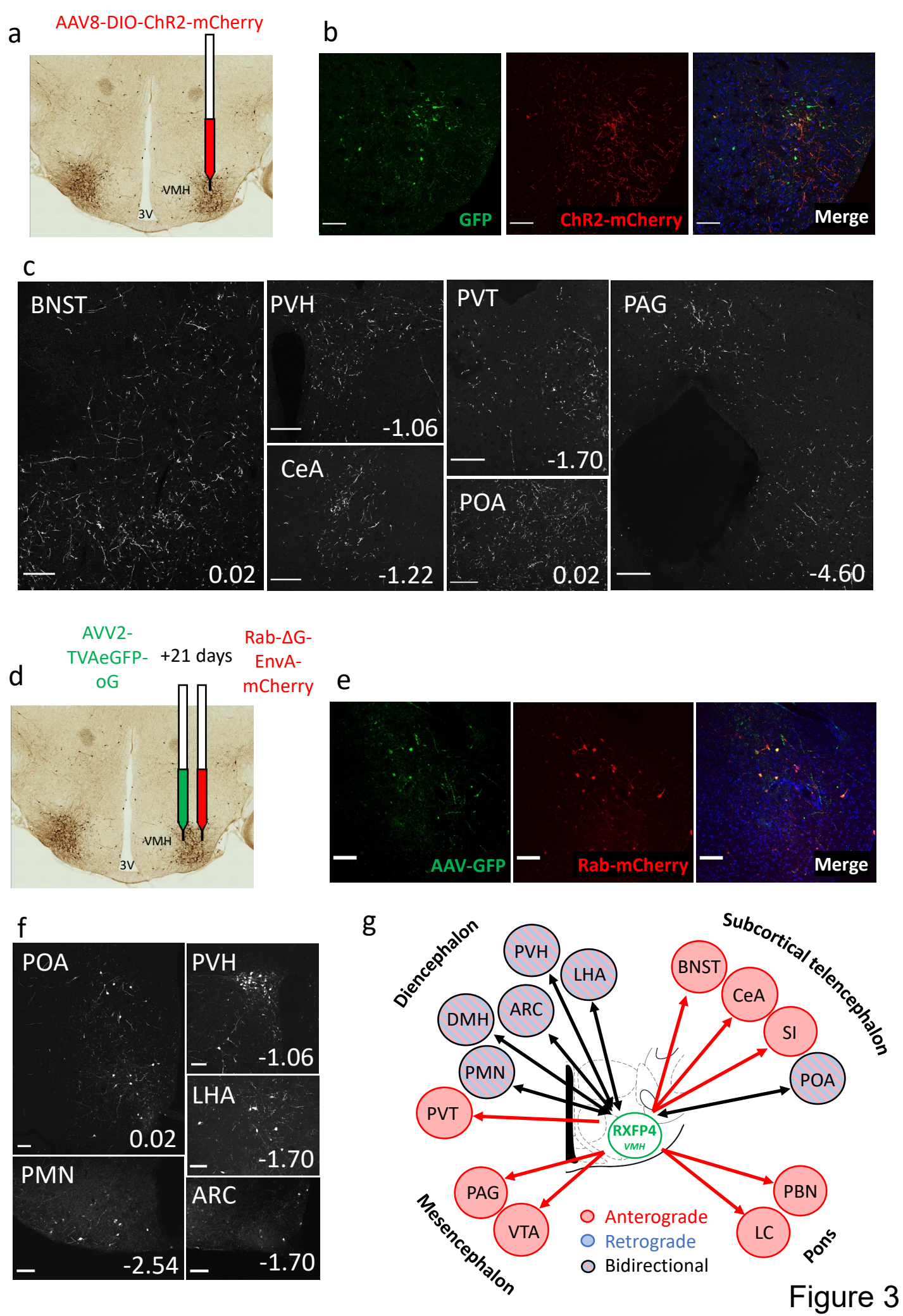
a
AAV8-DIO-ChR2-mCherry
VMH
3V
b
GFP
ChR2-mCherry
Merge
c
BNST
0.02
PVH
-1.06
CeA
-1.22
PVT
-1.70
POA
0.02
PAG
-4.60
d
AVV2-TVAeGFP-oG
+21 days
Rab-ΔG-EnvA-mCherry
VMH
3V
e
AAV-GFP
Rab-mCherry
Merge
f
POA
0.02
PVH
-1.06
LHA
-1.70
PMN
-2.54
ARC
-1.70
g
Diencephalon
Subcortical telencephalon
Mesencephalon
Pons
PVH
LHA
DMH
ARC
PMN
PVT
BNST
CeA
SI
POA
RXFP4
VMH
PAG
VTA
PBN
LC
Anterograde
Retrograde
Bidirectional

Figure 3

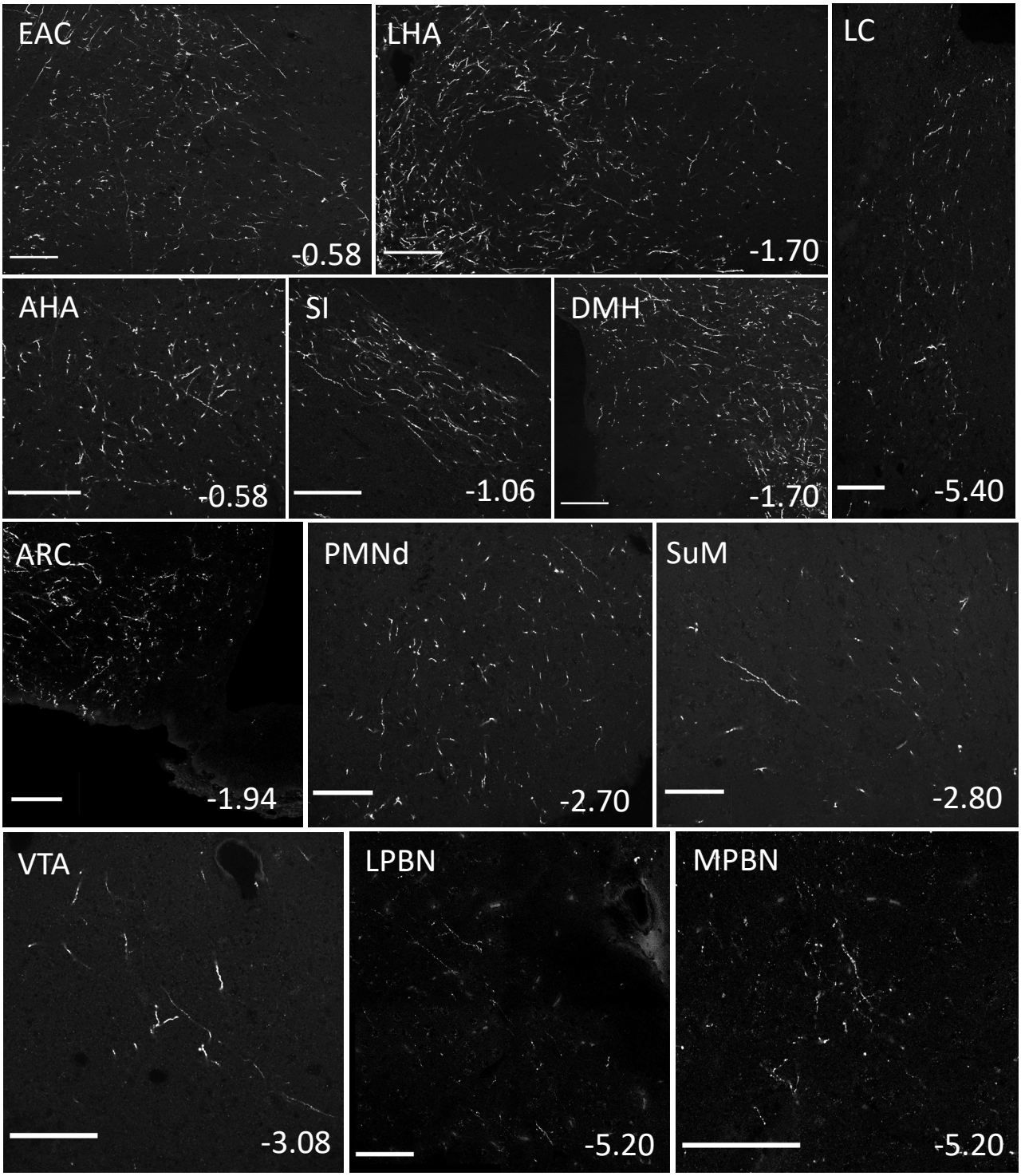

Supplementary Figure 3

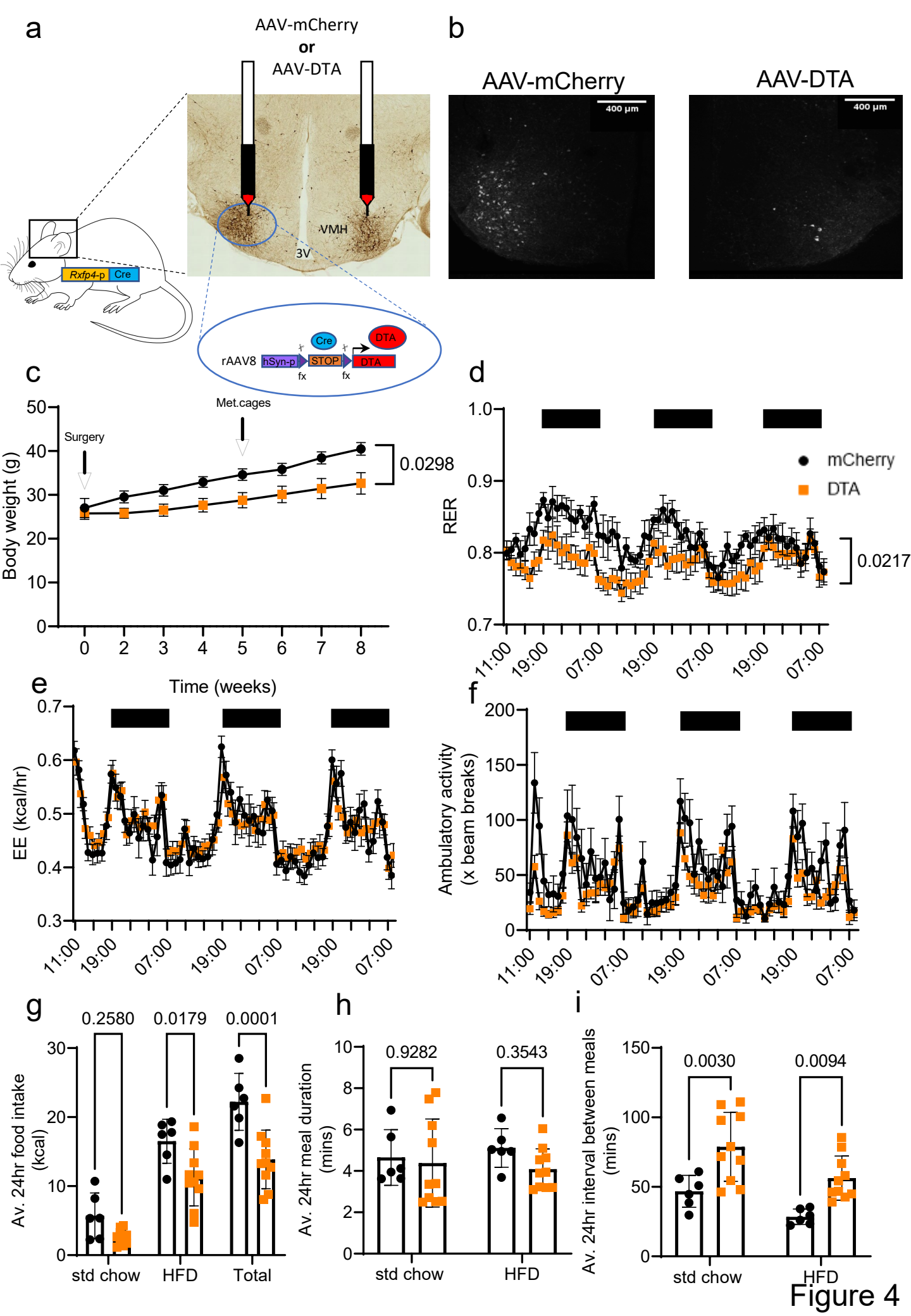
a
AAV-mCherry
or
AAV-DTA
VMH
3V
Rxfp4-p
Cre
rAAV8
hSyn-p
STOP
DTA
fx
b
AAV-mCherry
AAV-DTA
400 µm
c
Surgery
Met.cages
Body weight (g)
0.0298
Time (weeks)
d
RER
mCherry
DTA
0.0217
e
EE (kcal/hr)
f
Ambulatory activity
(x beam breaks)
g
0.2580
0.0179
0.0001
Av. 24hr food intake
(kcal)
std chow
HFD
Total
h
0.9282
0.3543
Av. 24hr meal duration
(mins)
i
0.0030
0.0094
Av. 24hr interval between meals
(mins)

Figure 4

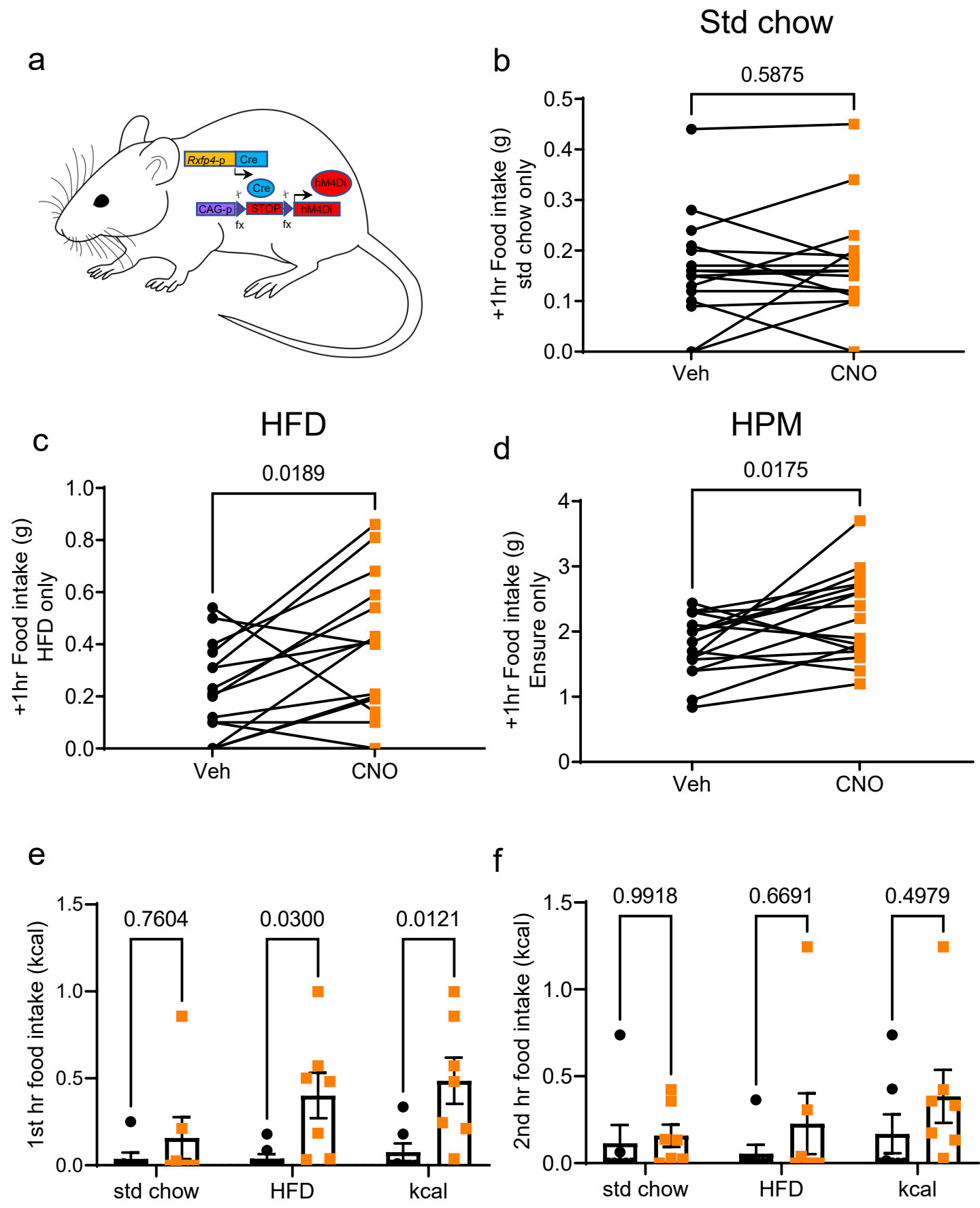
a
Rxfp4-p
Cre
Cre
hM4Di
CAG-p
STOP
hM4Di
fx
fx
b
Std chow
0.5875
+1hr Food intake (g)
std chow only
0.5
0.4
0.3
0.2
0.1
0.0
Veh
CNO
c
HFD
0.0189
+1hr Food intake (g)
HFD only
1.0
0.8
0.6
0.4
0.2
0.0
Veh
CNO
d
HPM
0.0175
+1hr Food intake (g)
Ensure only
4
3
2
1
0
Veh
CNO
e
0.7604
0.0300
0.0121
1st hr food intake (kcal)
1.5
1.0
0.5
0.0
std chow
HFD
kcal
f
0.9918
0.6691
0.4979
2nd hr food intake (kcal)
1.5
1.0
0.5
0.0
std chow
HFD
kcal

Figure 5

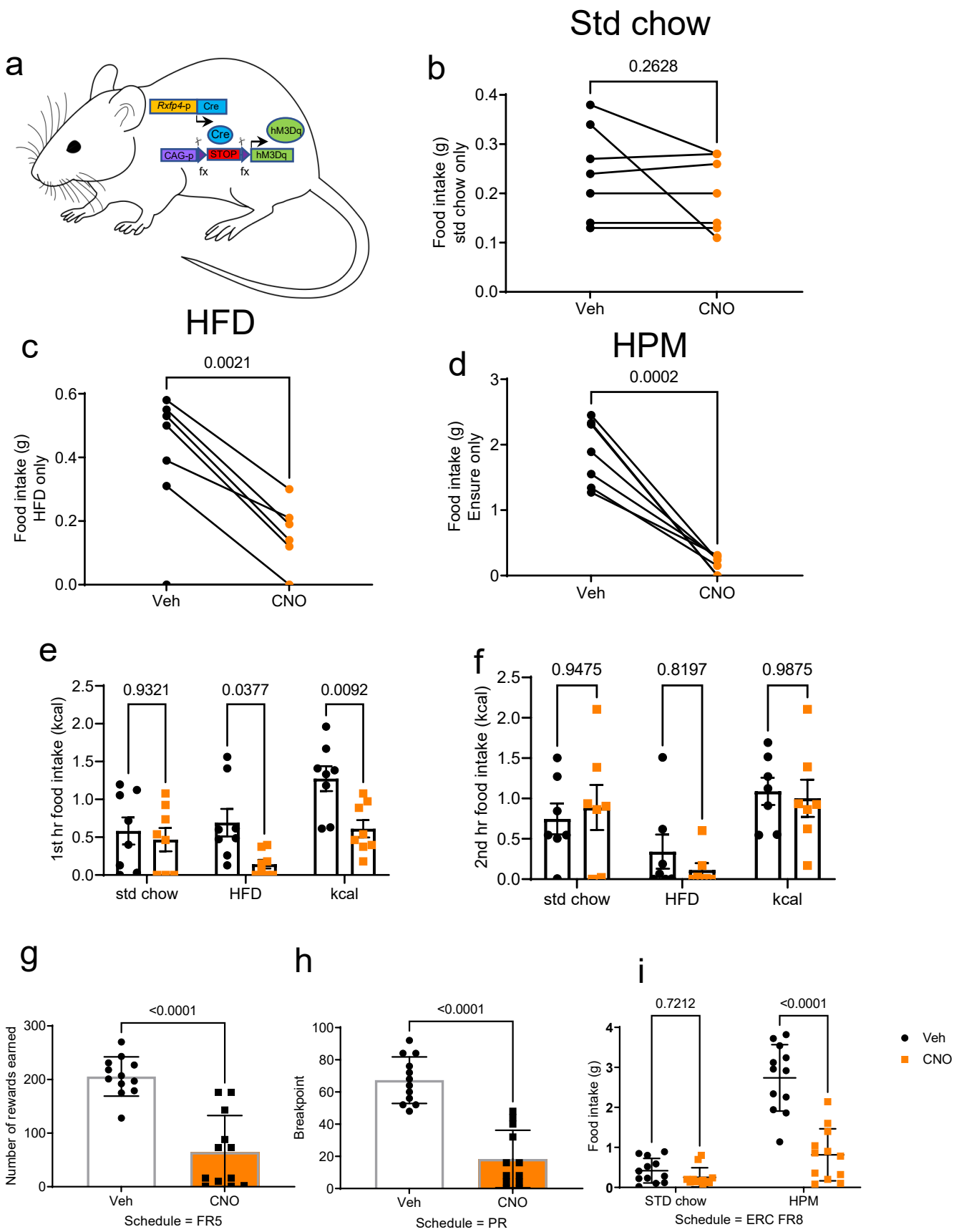

Link to videos

Figure 6

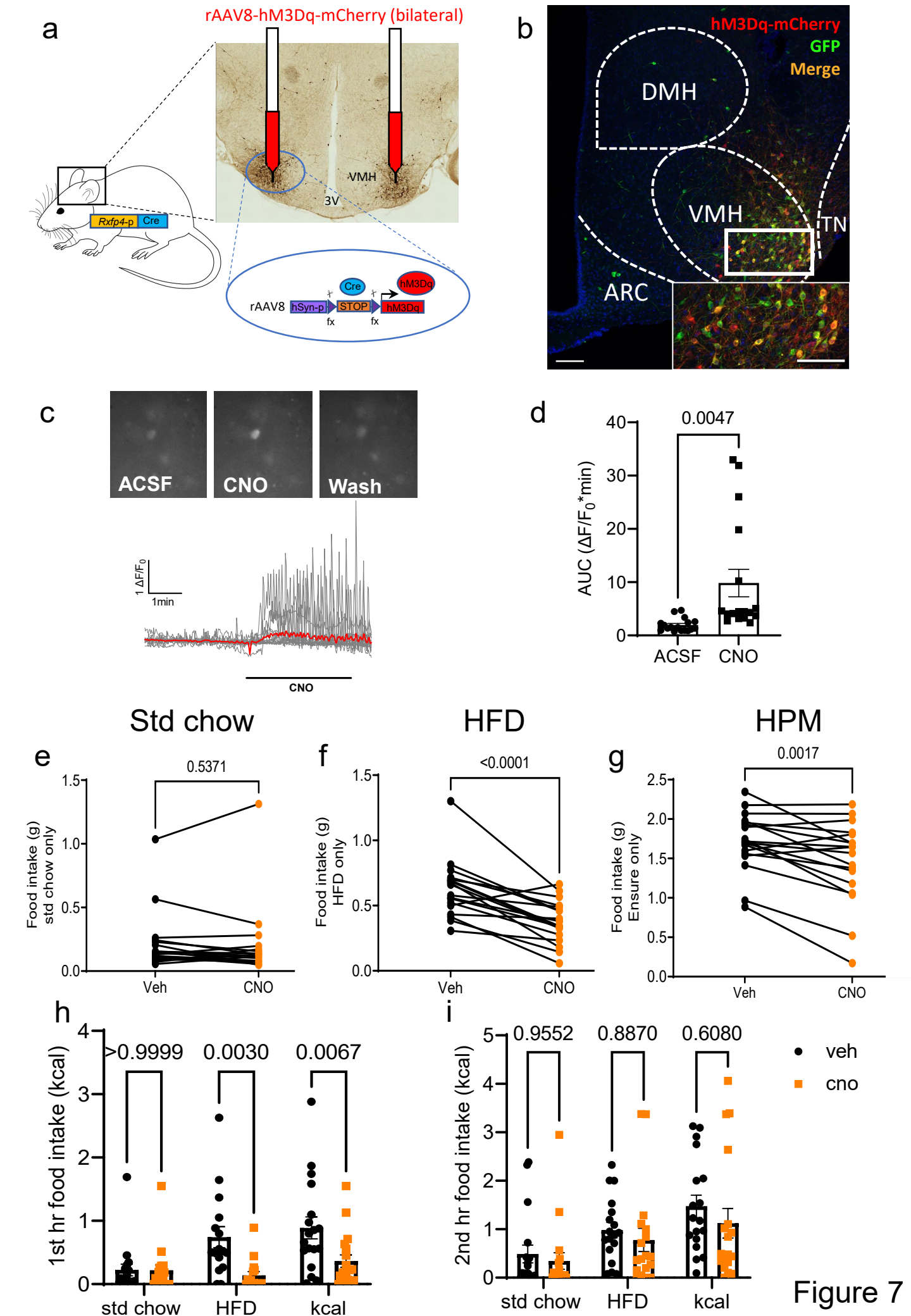
a
rAAV8-hM3Dq-mCherry (bilateral)
VMH
3V
Rxfp4-p
Cre
rAAV8
hSyn-p
STOP
hM3Dq
fx
b
hM3Dq-mCherry
GFP
Merge
DMH
VMH
TN
ARC
c
ACSF
CNO
Wash
1 ΔF/F0
1min
CNO
d
0.0047
AUC (ΔF/F0*min)
ACSF
CNO
Std chow
HFD
HPM
e
0.5371
Food intake (g) std chow only
Veh
CNO
f
<0.0001
Food intake (g) HFD only
g
0.0017
Food intake (g) Ensure only
h
>0.9999
0.0030
0.0067
1st hr food intake (kcal)
std chow
HFD
kcal
i
0.9552
0.8870
0.6080
2nd hr food intake (kcal)
veh
cno

Figure 7

RXFP4^{wb_Di}

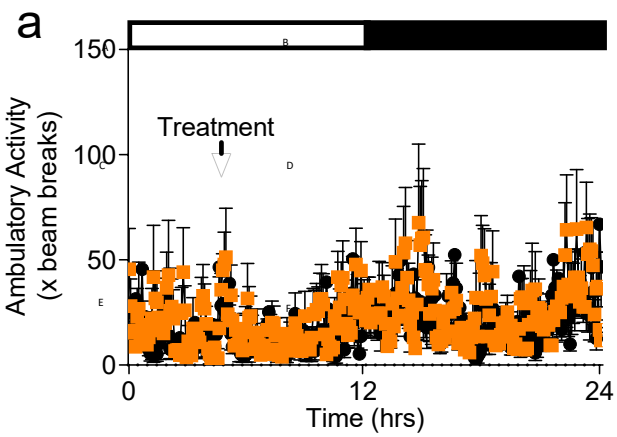

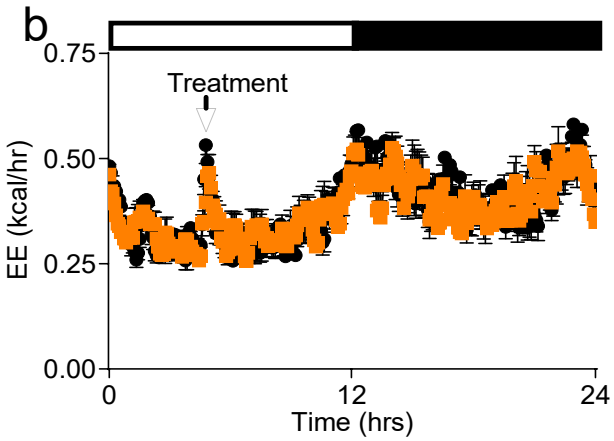

RXFP4$^{wb\text{-}Dq}$

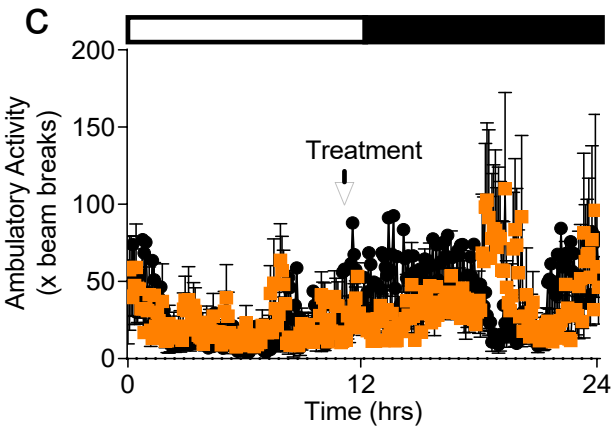

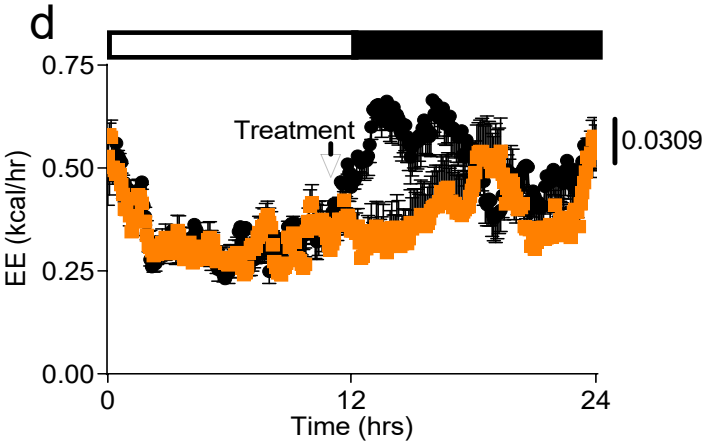

RXFP4^{VMHDq}

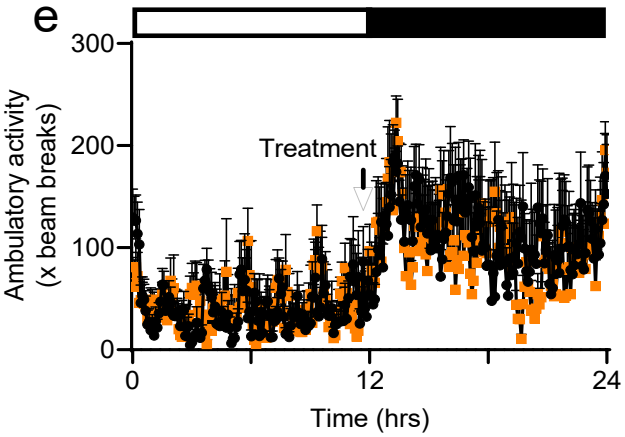

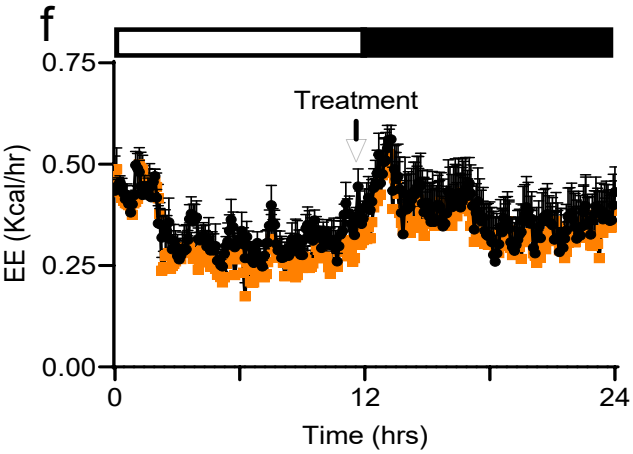

Supplementary Figure 4